Article:

Davies, CJ (2015) Cooling history of Earth's core with high thermal conductivity. Physics of the Earth and Planetary Interiors, 247. 65 - 79. ISSN: 0031-9201

https://doi.org/10.1016/j.pepi.2015.03.007

Cooling history of Earth's core with high thermal conductivity

Christopher J. Davies[a,b,*]

[a]*School of Earth and Environment, University of Leeds, Leeds LS2 9JT, UK*
[b]*Institute of Geophysics and Planetary Physics, Scripps Institution of Oceanography, University of California San Diego, 9500 Gilman Drive, La Jolla, CA 92093-0225*

Abstract

Thermal evolution models of Earth's core constrain the power available to the geodynamo process that generates the geomagnetic field, the evolution of the solid inner core and the thermal history of the overlying mantle. Recent upward revision of the thermal conductivity of liquid iron mixtures by a factor of 2–3 has drastically reduced the estimated power available to generate the present-day geomagnetic field. Moreover, this high conductivity increases the amount of heat that is conducted out of the core down the adiabatic gradient, bringing it into line with the highest estimates of present-day core-mantle boundary heat flow. These issues raise problems with the standard scenario of core cooling in which the core has remained completely well-mixed and relatively cool for the past 3.5 Ga. This paper presents cooling histories for Earth's core spanning the last 3.5 Ga to constrain the thermodynamic conditions corresponding to marginal dynamo evolution, i.e. where the ohmic dissipation remains just positive over time. The radial variation of core properties is represented by polynomials, which gives good agreement with radial profiles derived from seismological and mineralogical data and allows the governing energy and entropy equations to be solved analytically. Time-dependent evolution of liquid and solid light element concentrations, the melting curve and gravitational energy are calculated for an Fe-O-S-Si model of core chemistry. A suite of cooling histories are presented by varying the inner core boundary density jump, thermal conductivity and amount of radiogenic heat production in the core. All models where the core remains superadiabatic predict an inner core age of $\lesssim$600 Myr, about two times younger than estimates based on old (lower) thermal conductivity estimates, and core temperatures that exceed present estimates of the lower mantle solidus prior to the last 0.5–1.5 Ga. Allowing the top of the core to become strongly subadiabatic in recent times pushes the onset of inner core nucleation back to $\sim$1.5 Gyr, but the ancient core temperature still implies a partially molten mantle prior to $\sim$2 Ga. Based on these results, the scenario of a long-lived basal magma ocean and subadiabatic present-day core seems hard to avoid.

Keywords: Geodynamo, outer core, thermal history, inner core age

*Corresponding author
Email address: `c.davies@earth.leeds.ac.uk; tel: +44 (0) 113 3435543` (Christopher J. Davies)

1. Introduction

The paleomagnetic observation that the geomagnetic field has persisted for at least the last 3.45 Ga (Biggin et al., 2009; Tarduno et al., 2010) provides remarkable insight into the dynamics and evolution of Earth's deep interior. The field is generated in Earth's liquid outer core by a dynamo process in which the kinetic energy of fluid motions is converted into magnetic energy. The power source that keeps the core fluid moving is thought to derive from the slow cooling of the whole planet, and in particular the solid mantle, which sets the amount of heat flowing across the core-mantle boundary (CMB) (e.g. Gubbins et al., 1979). A viable cooling history for the Earth must involve sufficient CMB heat flow to power the geodynamo for the last ∼3.5 Ga. Moreover, the thermal evolution of the core places important constraints on the growth history of the solid inner core (e.g. Nimmo, 2007) and the evolution of the mantle (e.g. Buffett, 2002).

The standard procedure for calculating core cooling histories assumes that it is possible to average out rapid fluctuations associated with convection and the geodynamo process to leave equations describing the long-term evolution of the core (e.g. Gubbins et al., 1979; Braginsky and Roberts, 1995; Buffett et al., 1996; Labrosse et al., 1997; Gubbins et al., 2003). The outer core fluid, a mixture of iron together with some lighter elements, is supposed to be compositionally uniform and follow an adiabatic temperature profile as would be the case if it were vigorously convecting. The resulting model, which is employed in the present study, relates the CMB heat flow $Q_{\rm cmb}$, to the dissipation resulting from field generation, the Ohmic heating $E_{\rm J}$. The heat sources that make good the imposed CMB heat flow arise from the presence of any radiogenic elements in the core (e.g. Nimmo et al., 2004) and cooling by the mantle. Cooling leads to freezing of the solid inner core from the centre of the Earth outwards, which releases latent heat due to the phase change (Verhoogen, 1961) and leaves the light component of the iron mixture in the liquid phase where it is free to rise and provide a source of compositional buoyancy (Braginsky, 1963). Cooling also causes contraction of the core, but the associated heat sources are much smaller than those arising from inner core growth (Gubbins et al., 2003).

The relationship between $Q_{\rm cmb}$ and $E_{\rm J}$ depends on properties of the core fluid at the relevant pressure-temperature conditions. Advances in theoretical and experimental mineral physics techniques over the last few years have significantly improved estimates of core properties such as the melting temperature and composition (Alfè et al., 2007; Hirose et al., 2013). One quantity of particular importance is the thermal conductivity, k. Recent studies have presented the first calculations of k at core pressures and temperatures for both pure iron (Pozzo et al., 2012) and liquid iron mixtures (de Koker et al., 2012; Pozzo et al., 2013; Gomi et al., 2013). These studies used different techniques and yet all found k at the CMB in the range 80–110 W m^{-1} K^{-1}, increasing up to 140–160 W m^{-1} K^{-1} at the inner core boundary (ICB). These values are 2–3 times higher than those commonly found in the literature, e.g. $k = 28$ W m^{-1} K^{-1} (Stacey and Loper, 2007) and $k = 63$ W m^{-1} K^{-1} (Stacey and Anderson, 2001).

Nimmo (2007) summarises the results from core cooling models that used the old (low) values of thermal conductivity. The main conclusions are: 1) cooling can provide enough power to keep the core continually well-mixed and sustain the geomagnetic field over the last 3.5 Ga; 2) the inner core is a relatively young feature of the planet, around 1 billion years old; 3) the early core temperature was within the range of estimates for the lower mantle solidus. Remarkably, the seemingly innocuous change in k has raised significant problems with this picture.

Increasing the thermal conductivity enhances the heat $Q_{\mathrm{k}} = 4\pi k(r_{\mathrm{o}}) r_{\mathrm{o}}^2 \mathrm{d}T_{\mathrm{a}}/\mathrm{d}r|_{r=r_{\mathrm{o}}}$ that must be conducted across the CMB (radius $r = r_{\mathrm{o}}$) down the adiabatic gradient $\mathrm{d}T_{\mathrm{a}}/\mathrm{d}r|_{r=r_{\mathrm{o}}}$: for $k = 63$ W m^{-1} K^{-1} $Q_{\mathrm{k}} \approx 9$ TW while $k = 100$ W m^{-1} K^{-1} gives $Q_{\mathrm{k}} \approx 15$ TW (Pozzo et al., 2012). Here r is radius and T_{a} is the adiabatic temperature, defined below. Q_{cmb} is rather poorly known, even for the present-day. Using the range $Q_{\mathrm{cmb}} = 7-17$ TW estimated by Lay et al. (2009) and Nimmo (2014) implies that the top of the core is either neutrally stable ($Q_{\mathrm{cmb}} = Q_{\mathrm{k}}$) or subadiabatic ($Q_{\mathrm{cmb}} < Q_{\mathrm{k}}$). Subadiabatic conditions may give rise to stable stratification below the CMB (Labrosse et al., 1997; Lister and Buffett, 1998; Pozzo et al., 2012; Nakagawa and Tackley, 2013; Gomi et al., 2013), which has significant implications for explaining the geomagnetic secular variation because it precludes radial motion at the top of the core (e.g. Gubbins, 2007).

Heat conducted down the adiabat is not available to drive core convection and so increasing k also decreases the power available to the dynamo. Pozzo et al. (2012) found that maintaining the same magnetic field with the higher conductivity would require the core to cool roughly twice as rapidly, thus making the inner core a much younger feature of the planet, perhaps only 300 Myrs old. A younger inner core means that purely thermal convection, which is less efficient than chemically-driven convection (Lister and Buffett, 1995; Gubbins et al., 2004), must drive the geodynamo for longer. These issues have led to concerns that cooling at early times may not have been rapid enough to power the core dynamo (Buffett, 2012). Indeed, Ziegler and Stegman (2013) suggested that the early geomagnetic field may have been generated in a magma ocean at the base of the mantle. On the other hand, Nakagawa and Tackley (2014) found that the mantle cools the core too rapidly in some mantle convection models (the present-day inner core radius is smaller than the model prediction) and introduced a primordial layer of dense material at the base of the mantle in order to match the present-day ICB radius. The extent to which the new conductivity values modify previous conclusions regarding core thermal evolution is therefore rather uncertain at present. Resolving this issue is clearly fundamental to the basic model of long-term geodynamo evolution.

In this study we seek to constrain viable core thermal histories by searching for the conditions that give a marginal dynamo evolution, i.e. models with the minimum E_{J} such that $E_{\mathrm{J}} \geq 0$ for all time. The value of E_{J} for the geodynamo is probably much greater than zero (Roberts et al., 2003), but its value is very poorly known, partly because the toroidal component of the field does not emerge from the core and partly because the major contributions to E_{J} are thought to arise on small lengthscales (Gubbins, 1975). Lower values of E_{J} result in slower core cooling and so the models here are conservative in this sense. Attention is focused on the predicted inner core age, which is estimated to be 1 Gyr using old (low) thermal conductivity estimates (Labrosse et al., 2001), and the ancient core temperature. Estimates of the lower mantle solidus go from 3570±200 K (Nomura et al.,

2014) to ∼4150±150 K (e.g. Fiquet et al., 2010; Andrault et al., 2011). Core temperatures exceeding these values indicate partial melting of the lowermost mantle.

Most of the models in this study are constrained such that the whole core is superadiabatic ($Q_{\rm cmb} > Q_{\rm k}$). If $Q_{\rm cmb} < Q_{\rm k}$ a stable layer may develop below the CMB in which the assumptions of an adiabatic temperature profile and well-mixed light element concentration are not strictly valid. Instead, this situation requires the solution of conduction equations in the layer (Labrosse et al., 1997; Lister and Buffett, 1998). On the other hand, the whole core could remain adiabatic and well-mixed when $Q_{\rm cmb} < Q_{\rm k}$ if compositional convection can carry the excess heat downwards (Loper, 1978). Discriminating between the possibilities requires detailed analysis of the buoyancy sources that drive convection (Davies and Gubbins, 2011; Gomi et al., 2013), while the stability of the layer may be influenced by penetration of the underlying convection or double-diffusive instabilities (Manglik et al., 2010). Some models in this study correspond to a dynamo that is always marginal, which can cause the top of the core to become subadiabatic. We do not analyse the static stability of subadiabatic regions in these models and assume any stable regions that may form are thin enough not to influence the calculated entropy, i.e. that the assumptions of adiabaticity and well-mixed concentration continue to hold. Maintaining a given dissipation requires the core to cool faster if a stable region is present, implying younger inner core ages and higher ancient core temperatures than those estimated below.

This paper is organised as follows. In section 2 we outline the model equations and define a new polynomial representation of the radial core structure that is designed to give good agreement with present-day profiles derived from seismological and mineralogical data. We also describe a method to compute the depression of the pure iron melting point due to the presence of multiple light element species. The proposed radial core structure and melting curve are compared to previous studies in section 3. In section 4 we present a selection of core cooling models by varying the most uncertain input parameters: the density jump at the ICB, the thermal conductivity and the amount of radiogenic heating. Discussion and conclusions are presented in section 5. The main result of this work is contained in Figure 7.

2. Methods

The governing equations describing global energy and entropy balance have been described in detail elsewhere (Gubbins et al., 2003, 2004; Nimmo, 2014) and only an outline is given here. The equivalence of alternative formulations (e.g. Buffett et al., 1996; Labrosse et al., 1997) to the present model was shown by Lister (2003). Averaging over a timescale that is long compared to the timescale associated with fluctuations of the dynamo process but short compared to the evolutionary timescale of the core it is assumed that convection mixes the outer core to a basic state of hydrostatic equilibrium, uniform composition ($\nabla c^l_X = 0$ where c^l_X is the mass concentration of light impurity X in the liquid), and an adiabatic temperature $T_{\rm a}(r)$. Radial variation of thermodynamic properties are supposed to far exceed lateral variations (Stevenson, 1987) and so all variables are assumed to vary only in radius r with $r_{\rm o}$ the CMB and $r_{\rm i}(t)$ the ICB, which changes in time t as the inner core grows. These approximations are also taken to hold in the inner core. Although the viability of inner core convection is currently the subject of debate (see Buffett, 2009; Pozzo et al., 2014, for a discussion), Labrosse et al. (1997) suggest that this assumption has only a minor effect on the results. With these approximations, the energy balance can be written (Gubbins et al., 2003, 2004)

$$\begin{aligned}\underbrace{-\oint k\nabla T\cdot\mathbf{n}\mathrm{d}S}_{Q_{\mathrm{cmb}}} = & \underbrace{-\frac{C_p}{T_{\mathrm{o}}}\int\rho T_{\mathrm{a}}\mathrm{d}V\frac{\mathrm{d}T_{\mathrm{o}}}{\mathrm{d}t}}_{Q_{\mathrm{s}}}\underbrace{-4\pi r_{\mathrm{i}}^2 L\rho_{\mathrm{i}}C_r\frac{\mathrm{d}T_{\mathrm{o}}}{\mathrm{d}t}}_{Q_{\mathrm{L}}}+\underbrace{\alpha_c\frac{Dc_X^l}{Dt}\int\rho\psi\mathrm{d}V}_{Q_{\mathrm{g}}} \\ & +\underbrace{\int\alpha_T T_{\mathrm{a}}\frac{DP}{Dt}\mathrm{d}V}_{Q_{\mathrm{P}}}+\underbrace{4\pi r_{\mathrm{i}}^2 L\rho_{\mathrm{i}}C_r\frac{\mathrm{d}T_{\mathrm{m}}}{\mathrm{d}P}\frac{DP}{Dt}}_{Q_{\mathrm{PL}}}+\underbrace{\int\rho h\mathrm{d}V}_{Q_{\mathrm{r}}},\end{aligned} \tag{1}$$

where

$$\frac{Dc_X^l}{Dt}=\frac{4\pi r_{\mathrm{i}}^2\rho_{\mathrm{i}}}{M_{\mathrm{oc}}}C_r\left(c_X^l-c_X^s\right)\frac{\mathrm{d}T_{\mathrm{o}}}{\mathrm{d}t} \tag{2}$$

and

$$C_r=\frac{1}{(\mathrm{d}T_m/\mathrm{d}P)_{r=r_{\mathrm{i}}}-(\partial T_{\mathrm{a}}/\partial P)_{r=r_{\mathrm{i}}}}\frac{1}{\rho_{\mathrm{i}}g_{\mathrm{i}}}\frac{T_{\mathrm{i}}}{T_{\mathrm{o}}}. \tag{3}$$

Here the density $\rho(r)$, gravity $g(r)$, gravitational potential $\psi(r)$, pressure $P(r)$, thermal expansion coefficient α_T and melting temperature $T_{\mathrm{m}}(r)$ are functions of r and subscripts i and o refer to quantities evaluated at r_{i} and r_{o} respectively. In writing equation (1) the CMB has been assumed to be insulating, and the specific heat capacity at constant pressure C_p, compositional expansion coefficient $\alpha_c=\rho^{-1}(\partial\rho/\partial c_X)_{P,T}$ and latent heat L have been assumed constant. All other parameters are defined in Table 1. In writing equation (2) it has been assumed that the concentration of element X in the solid, c_X^s, does not vary in time. This is shown to be a good approximation in Figure 6 below. Note that Q_{cmb} contains the total temperature T rather than the adiabatic temperature. $\mathbf{n}$ is the outward normal to the surface S, which encloses the volume V of the core; V_{oc} is the volume of the outer core.

Equation (1) states that the total CMB heat flow Q_{cmb} is balanced by heat released from cooling the core Q_{s}, latent heat release due to the phase change at the ICB Q_{L}, gravitational energy due to the segregation of light elements into the liquid phase on freezing Q_{g}, heat released due to slow contraction of the core $Q_{\mathrm{P}}+Q_{\mathrm{PL}}$ and radiogenic heating Q_{r}. It describes the thermal evolution of the core but does not explicitly contain the magnetic field $\mathbf{B}$ and hence does not say anything about maintaining the geodynamo. $\mathbf{B}$ does appear in the entropy balance, which can be written (Gubbins et al., 2003, 2004)

$$
\begin{aligned}
\underbrace{\frac{1}{\mu_0^2}\int \frac{(\nabla \times \mathbf{B})^2}{T_\mathrm{a}\sigma}\mathrm{d}V}_{E_\mathrm{J}} \quad + \quad & \underbrace{\int k\left(\frac{\nabla T_\mathrm{a}}{T_\mathrm{a}}\right)^2 \mathrm{d}V}_{E_\mathrm{k}} + \underbrace{\alpha_c^2\alpha_D\int\frac{g^2}{T_\mathrm{a}}\mathrm{d}V}_{E_\mathrm{a}} \\
= \quad & \underbrace{\frac{C_p}{T_\mathrm{o}}\left(M_\mathrm{c} - \frac{1}{T_\mathrm{o}}\int \rho T_\mathrm{a}\mathrm{d}V\right)\frac{\mathrm{d}T_\mathrm{o}}{\mathrm{d}t}}_{E_\mathrm{s}} \underbrace{-Q_\mathrm{L}\frac{(T_\mathrm{i}-T_\mathrm{o})}{T_\mathrm{i}T_\mathrm{o}}}_{E_\mathrm{L}} + \underbrace{\frac{Q_\mathrm{g}}{T_\mathrm{o}}}_{E_\mathrm{g}} + \\
& \underbrace{\frac{Q_\mathrm{P}}{T_\mathrm{o}} - \int \alpha_T\frac{DP}{Dt}\mathrm{d}V}_{E_\mathrm{P}} + \underbrace{Q_\mathrm{PL}\left(\frac{1}{T_\mathrm{o}} - \frac{1}{T_\mathrm{i}}\right)}_{E_\mathrm{PL}} + \\
& \underbrace{h\left(\frac{M_\mathrm{c}}{T_\mathrm{o}} - \int\frac{\rho}{T_\mathrm{a}}\mathrm{d}V\right)}_{E_\mathrm{r}} \underbrace{-\frac{Dc_X^l}{Dt}\int\rho\left(\frac{\partial\mu}{\mathrm{d}T}\right)_{P,c}\mathrm{d}V_\mathrm{oc}}_{E_\mathrm{h}}
\end{aligned}
\tag{4}
$$

This equation shows that three positive definite sources of entropy, the Ohmic heating E_J, entropy of thermal conduction E_k, and the entropy of molecular diffusion of light elements E_a, balance entropy production associated with secular cooling E_s, gravitational energy release E_g, latent heat release E_L, contraction $E_\mathrm{P} + E_\mathrm{PL}$, radiogenic heating E_r and heat of reaction E_h. Here the viscous dissipation, which is supposed to be small in the core (Gubbins et al., 2003), has been neglected. Note that the definition of heat of reaction differs from that given in Gubbins et al. (2004); this issue was identified by F. Nimmo (pers comms).

Equations (1) and (4) can be written in the compact form (Gubbins et al., 2004; Nimmo, 2007)

$$
\begin{aligned}
Q_\mathrm{cmb} = \quad & \left(\tilde{Q}_\mathrm{s} + \tilde{Q}_\mathrm{L} + \tilde{Q}_\mathrm{g} + \tilde{Q}_\mathrm{P} + \tilde{Q}_\mathrm{PL}\right)\frac{\mathrm{d}T_\mathrm{o}}{\mathrm{d}t} + \tilde{Q}_\mathrm{r}h, \\
E_\mathrm{J} + E_\mathrm{k} + E_\mathrm{a} = \quad & \left(\tilde{E}_\mathrm{s} + \tilde{E}_\mathrm{L} + \tilde{E}_\mathrm{g} + \tilde{E}_\mathrm{P} + \tilde{E}_\mathrm{PL} + \tilde{E}_\mathrm{h}\right)\frac{\mathrm{d}T_\mathrm{o}}{\mathrm{d}t} + \tilde{E}_\mathrm{r}h,
\end{aligned}
\tag{5}
$$

where $Q_\mathrm{L} = \tilde{Q}_\mathrm{L}(\mathrm{d}T_\mathrm{o}/\mathrm{d}t)$ and similarly for other terms. The tilde quantities can be calculated using knowledge of the radial variation of core properties. Equations (5) show that knowledge of the CMB heat-flux Q_cmb and the amount of radiogenic heat production per unit mass h determines the cooling rate of the core $\mathrm{d}T_\mathrm{o}/\mathrm{d}t$ and hence the Ohmic heating E_J. E_J can be related to the gravitational energy that drives convective motion (Buffett et al., 1996) and hence represents the fraction of the input energy that ends up doing useful work by generating magnetic field. $\mathrm{d}T_\mathrm{o}/\mathrm{d}t$ is also related to the growth rate of the inner core, $\mathrm{d}r_\mathrm{i}/\mathrm{d}t$, by (Gubbins et al., 2003)

$$
\frac{\mathrm{d}r_\mathrm{i}}{\mathrm{d}t} = C_r\frac{\mathrm{d}T_\mathrm{o}}{\mathrm{d}t}. \tag{6}
$$

Equally, specifying E_J and h determines $\mathrm{d}T_\mathrm{o}/\mathrm{d}t$ and Q_cmb. Owing to the significant uncertainties in E_J and Q_cmb, both approaches are considered in this work.

It should be noted that equations (1) and (4) do not explicitly contain the fluid velocity. The fact that the core is vigorously convecting is implicit in the formulation because it is assumed that this convection maintains an adiabatic and compositionally uniform state when short timescale phenomena are averaged out. The main product of the geodynamo process, $\mathbf{B}$, appears in the entropy balance although it does not need to be evaluated explicitly because determining E_{J} is enough to assess the viability of dynamo action. Therefore, equations (5) allow the long-term evolution of the core to be determined without requiring detailed knowledge of the fluid flow or magnetic field.

The following sections describe the expressions used to evaluate the integrals in equations (1) and (4) and the model of core chemistry. The term "core structure" is used to refer to the radial variation of core properties.

2.1. Core structure

The radial variation of $\rho(r)$, $g(r)$, $\psi(r)$, $P(r)$, $T_{\mathrm{m}}(r)$, $T_{\mathrm{a}}(r)$ and $k(r)$ is approximated by polynomials, which allows the integrals in equations (1) and (4) to be written analytically. The form of the expressions is chosen primarily to fit observational data rather than from theoretical considerations. Present-day core structure is now fairly well-known. Unfortunately, information on past core structure is almost non-existent. Cooling on the adiabat is independent of position to a good approximation (Gubbins et al., 2003), suggesting that past and present adiabatic profiles will be similar. Indeed, the cooling contribution to other fields (density, etc) should also not significantly affect the time variation of their radial profiles. Contraction could change the radial variation of core properties, but these effects are small for the present-day (Gubbins et al., 2003) and are shown below to make a small contribution to the long-term core evolution. We therefore take the view that obtaining a good fit to present-day core structure is of particular importance. Alternative expressions for radial core structure have been used in previous studies (e.g. Labrosse et al., 1997; Nimmo, 2014) and these will be discussed in section 3.

2.1.1. Density

Core density is taken from the Preliminary Reference Earth Model (PREM) (Dziewonski and Anderson, 1981). Dziewonski and Anderson (1981) give a polynomial fit to the PREM density data, which can be written as

$$\begin{aligned} \rho(r) = & \qquad\qquad \rho_0^{\mathrm{ic}} + \rho_2^{\mathrm{ic}} r^2 & 0 \le r \le r_{\mathrm{i}}, \\ = & \ \rho_0^{\mathrm{oc}} + \rho_1^{\mathrm{oc}} r + \rho_2^{\mathrm{oc}} r^2 + \rho_3^{\mathrm{oc}} r^3 & r_{\mathrm{i}} \le r \le r_{\mathrm{o}}, \end{aligned} \tag{7}$$

where the ρ_i^{oc} are coefficients evaluated from a least squares fit of (7) to the outer core PREM density data and ρ_i^{ic} are similar coefficients for the inner core. This expression for ρ accounts for the density jump at the ICB.

With this definition of ρ the mass of the inner core is

$$M_{\mathrm{ic}} = 4\pi \int_0^{r_{\mathrm{i}}} \rho r^2 \mathrm{d}r = 4\pi \left[\frac{\rho_0^{\mathrm{ic}} r_{\mathrm{i}}^3}{3} + \frac{\rho_2^{\mathrm{ic}} r_{\mathrm{i}}^5}{5} \right] \tag{8}$$

and the mass of the outer core is

$$
\begin{aligned}
M_{\rm oc} &= 4\pi \int_{r_{\rm i}}^{r_{\rm o}} \rho r^2 {\rm d}r \\
&= 4\pi \left[\frac{\rho_0^{\rm oc} r_{\rm o}^3}{3} + \frac{\rho_1^{\rm oc} r_{\rm o}^4}{4} + \frac{\rho_2^{\rm oc} r_{\rm o}^5}{5} + \frac{\rho_3^{\rm oc} r_{\rm o}^6}{6} - \left(\frac{\rho_0^{\rm oc} r_{\rm i}^3}{3} + \frac{\rho_1^{\rm oc} r_{\rm i}^4}{4} + \frac{\rho_2^{\rm oc} r_{\rm i}^5}{5} + \frac{\rho_3^{\rm oc} r_{\rm i}^6}{6} \right) \right]. \quad (9)
\end{aligned}
$$

The mass of the whole core $M_{\rm c} = M_{\rm ic} + M_{\rm oc}$. The variation of gravity g across the inner core is given by

$$
g(r) = \frac{4\pi G}{r^2} \int_0^r \rho r'^2 {\rm d}r' = 4\pi G \left[\frac{\rho_0^{\rm ic} r}{3} + \frac{\rho_2^{\rm ic} r^3}{5} \right] \qquad 0 \le r \le r_{\rm i}. \quad (10)
$$

Denoting $g(r_{\rm i})$ by $g_{\rm i}^-$ in equation (10) the variation of g across the outer core is

$$
g(r) = 4\pi G \left(\frac{\rho_0^{\rm oc} r}{3} + \frac{\rho_1^{\rm oc} r^2}{4} + \frac{\rho_2^{\rm oc} r^3}{5} + \frac{\rho_3^{\rm oc} r^4}{6} - \left[\frac{\rho_0^{\rm oc} r_{\rm i}^3}{3r^2} + \frac{\rho_1^{\rm oc} r_{\rm i}^4}{4r^2} + \frac{\rho_2^{\rm oc} r_{\rm i}^5}{5r^2} + \frac{\rho_3^{\rm oc} r_{\rm i}^6}{6r^2} \right] \right) + \left(\frac{r_{\rm i}^2}{r^2} \right) g_{\rm i}^- . \quad (11)
$$

Equations (10) and (11) preserve continuity of g across the ICB.

The variation of the gravitational potential across the outer core is needed to evaluate the $Q_{\rm g}$ terms in equations (5). Relative to zero potential at the CMB it is

$$
\begin{aligned}
\psi(r) = -\int_r^{r_{\rm o}} g {\rm d}r' &= 4\pi G \left(\left[\frac{\rho_0^{\rm oc} r^2}{6} + \frac{\rho_1^{\rm oc} r^3}{12} + \frac{\rho_2^{\rm oc} r^4}{20} + \frac{\rho_3^{\rm oc} r^5}{30} \right]_{r_{\rm o}}^{r} - \right. \quad (12) \\
&\left. \left[\frac{\rho_0^{\rm ic} r_{\rm i}^3}{3r} + \frac{\rho_2^{\rm ic} r_{\rm i}^5}{5r} \right]_{r_{\rm o}}^{r} + \left[\frac{\rho_0^{\rm oc} r_{\rm i}^3}{3r} + \frac{\rho_1^{\rm oc} r_{\rm i}^4}{4r} + \frac{\rho_2^{\rm oc} r_{\rm i}^5}{5r} + \frac{\rho_3^{\rm oc} r_{\rm i}^6}{6r} \right]_{r_{\rm o}}^{r} \right).
\end{aligned}
$$

In both equations (11) and (12) the second and third terms in square brackets arise from the ICB density jump. These terms make a maximum contribution of 2% to the value of $g(r)$ and 0.5% to $\psi(r)$, as shown in Figure 1. The gravity profile is needed to obtain the pressure, but neglecting the contribution from the density jump gives a $P(r)$ [equation (13)] that differs by at most 1% from the PREM pressure. $g(r_{\rm i})$ is needed in equation (3); however, as g is continuous across the ICB, $g(r_{\rm i})$ can also be obtained from equation (10), which matches PREM to within a fraction of a percent. The gravitational potential profile is needed to evaluate $Q_{\rm g}$, but neglecting the contribution to $\psi(r)$ from the density jump gives an answer that is very close to previous studies (section 3). We therefore neglect the contributions to $g(r)$ and $\psi(r)$ from the ICB density jump and use the profiles shown by solid lines in Figure 1.

The pressure variation is obtained from the hydrostatic equation. Across the inner core

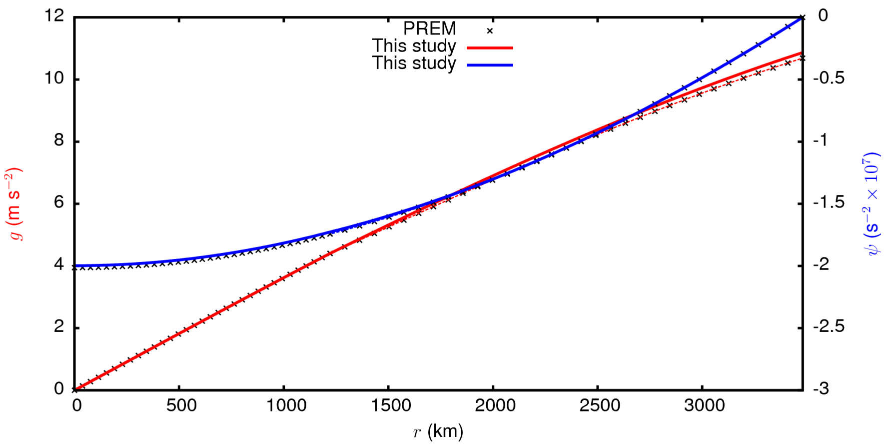

Figure 1: Radial variation of gravity g (left ordinate) and gravitational potential ψ (right ordinate). Crosses denote g and ψ obtained from PREM. Dashed lines show the polynomial expressions in equations (10), (11) and (12); solid lines use these equations but omitting the terms that arise from the ICB density jump.

it is given by

$$
\begin{aligned}
P(r) \;=\; & \int_r^{r_\mathrm{o}} \rho g \mathrm{d}r' = -4\pi G \left[\frac{\rho_0^{\mathrm{oc}^2}}{6} r^2 + \frac{7\rho_0^{\mathrm{oc}}\rho_1^{\mathrm{oc}}}{36} r^3 + \left(\frac{2\rho_0^{\mathrm{oc}}\rho_2^{\mathrm{oc}}}{15} + \frac{\rho_1^{\mathrm{oc}^2}}{16} \right) r^4 + \right. \\
& \left. \left(\frac{\rho_0^{\mathrm{oc}}\rho_3^{\mathrm{oc}}}{10} + \frac{9\rho_1^{\mathrm{oc}}\rho_2^{\mathrm{oc}}}{100} \right) r^5 + \left(\frac{5\rho_1^{\mathrm{oc}}\rho_3^{\mathrm{oc}}}{72} + \frac{\rho_2^{\mathrm{oc}^2}}{30} \right) r^6 + \frac{11\rho_2^{\mathrm{oc}}\rho_3^{\mathrm{oc}}}{210} r^7 + \frac{\rho_3^{\mathrm{oc}^2}}{42} r^8 \right]_{r_\mathrm{i}}^{r_\mathrm{o}} \qquad (13) \\
& + P_\mathrm{o} - 4\pi G \left[\frac{\rho_0^{\mathrm{ic}^2}}{6} r^2 + \frac{2\rho_0^{\mathrm{ic}}\rho_2^{\mathrm{ic}}}{15} r^4 + \frac{\rho_2^{\mathrm{ic}^2}}{30} r^6 \right]_r^{r_\mathrm{i}},
\end{aligned}
$$

where P_o is the pressure at the CMB. The pressure variation across the outer core is obtained by setting the term in the second square bracket to zero and putting r instead of r_i in the lower limit of the term in the first square bracket.

2.1.2. Temperature

The adiabatic temperature satisfies the equation

$$
T_\mathrm{a}(r) = T_\mathrm{cen} \exp\left(- \int_0^r \frac{g\gamma}{\phi} \mathrm{d}r \right), \qquad (14)
$$

where T_cen is the temperature at the centre of the Earth, γ is the Grüneisen parameter and ϕ is the seismic parameter. Here we approximate equation (14) by the polynomial

$$
T_\mathrm{a}(r) = T_\mathrm{cen}(1 + t_1 r + t_2 r^2 + t_3 r^3). \qquad (15)
$$

Values for the coefficients t_i are obtained from a least-squares fit to equation (14) using $\gamma \approx 1.5$ independent of radius (e.g. Gubbins et al., 2003; Stacey, 2007) and ϕ and g from

PREM. The coefficient $T_{\rm cen}$ is set by the requirement that $T_{\rm a}$ equals the melting temperature of the core mixture at the ICB.

We use the melting point data for pure iron from Alfè et al. (2002c). These data are fit with a polynomial of the form

$$T_{\rm m,Fe}(P) = t_{\rm m0}(1 + t_{\rm m1}P + t_{\rm m2}P^2 + t_{\rm m3}P^3), \tag{16}$$

where values for the coefficients $t_{\rm m\it i}$ are found from a least squares fit to the melting point data.

The entropy of melting for pure iron $\Delta S_{\rm Fe}$ is written as

$$\Delta S_{\rm Fe}(P) = S_1 + S_2P + S_3P^2 + S_4P^3, \tag{17}$$

where the coefficients S_i are obtained by fitting equation (17) to the data of Alfè et al. (2002c). Note that the data of Alfè et al. (2002c) is given in units of the Boltzmann constant and so equation (17) is also written in these units. $\Delta S_{\rm Fe}$ is used to determine the depression of the melting point by light impurities below.

2.1.3. Core chemistry

The ICB density jump, $\Delta\rho$, arises partly because solid core material is denser than liquid core material at the same pressure-temperature conditions and partly because the outer core is enriched in light elements compared to the inner core (Poirier, 1994). The ICB density jump therefore determines the relative importance of compositional and thermal convection and is a crucial input parameter. Unfortunately $\Delta\rho$ is uncertain by about 25%. Moreover, although geochemical constraints are available, the actual elements are very poorly known (see Nimmo, 2007, for a discussion) and so a candidate model of core chemistry must specify the elements as well as their abundances subject to the constraints that the model density profile matches the observed core density profile, including the jump at the ICB, together with the mass of the core.

This study utilises two models of core chemistry (Alfè et al., 2002b, 2007) that satisfy the constraints stated above. The first, hereafter labelled model PREM, has $\Delta\rho = 0.6$ g cm^{-1} (Dziewonski and Anderson, 1981); it consists of an iron inner core with 10% S and/or Si and an outer core with 8.5% S and/or Si plus an additional 8% O. The second, hereafter labelled model MG, has $\Delta\rho = 0.8$ g cm^{-1} (Masters and Gubbins, 2003); it consists of an iron inner core with 8% S and/or Si and an outer core with the same mixture plus an additional 13% O. Alfè et al. (2002b) find that S and Si partition almost equally between the inner and outer cores, while O partitions almost entirely into the liquid; it is therefore O that is mainly responsible for the compositional part of the ICB density jump in these models. The contributions of all three elements to the gravitational terms $Q_{\rm g}$ and $E_{\rm g}$ and to the entropy of molecular diffusion $E_{\rm a}$ are calculated separately and combined by simple addition.

The presence of a light element X in the core depresses the melting temperature of pure iron by an amount $\Delta T_{\rm X}$. The intersection of the melting curve and the adiabat determines the ICB radius and so the melting point depression is an important parameter. $\Delta T_{\rm X}$ depends on the concentration of X in the liquid and solid. Gubbins et al. (2013) showed how to obtain the solid concentration from the liquid concentration for O, and (Labrosse, 2014) performed the calculation for S. Here we extend this work to calculate the partitioning of Si and use these results to obtain the melting point depression due to O, S and Si. As in Labrosse (2014) and Alfè et al. (2002b) we assume that the concentrations of the various species evolve independently of each other. It is convenient to use molar rather than mass concentrations, which will be denoted by an overbar. The equations needed to convert between molar and mass concentrations are given by Labrosse (2014).

According to the theory of Alfè et al. (2002a), ΔT_X^m is given by

$$\Delta T_{\mathrm{X}} = \frac{T_{\mathrm{m,Fe}}}{\Delta S_{\mathrm{Fe}}}\left(\bar{c}_X^s - \bar{c}_X^l\right). \tag{18}$$

An equation for $\bar{c}_X^s$ can be obtained from the condition for thermodynamic equilibrium at the ICB, which requires that the chemical potentials of the solid and liquid be equal (Alfè et al., 2002a). This condition can be written

$$\mu_0^l + \lambda^l \bar{c}_X^l + k_B T_{\mathrm{m}} \ln \bar{c}_X^l = \mu_0^s + \lambda^s \bar{c}_X^s + k_B T_{\mathrm{m}} \ln \bar{c}_X^s, \tag{19}$$

where μ_0^l and μ_0^s are the (constant) chemical potentials for the liquid and solid respectively, λ^l and λ^s are constants representing corrections to the μ_0 terms (Alfè et al., 2002a), and k_B is Boltzmann's constant. Assuming that each light element makes an independent contribution to the melting temperature T_{m} of the mixture we can substitute $T_{\mathrm{m}} = T_{\mathrm{m,Fe}} + \Delta T_{\mathrm{X}}$ into equation (19) and obtain a transcendental equation that must be solved for $\bar{c}_X^s$:

$$\Delta\mu_0 + \lambda^l \bar{c}_X^l - \lambda^s \bar{c}_X^s - k_B T_{\mathrm{m,Fe}} \ln\left(\frac{\bar{c}_X^s}{\bar{c}_X^l}\right)\left(1 + \frac{(\bar{c}_X^s - \bar{c}_X^l)}{\Delta S_{\mathrm{Fe}}}\right) = 0, \tag{20}$$

where $\Delta\mu_0 = \mu_0^l - \mu_0^s$. For an initial value of $\bar{c}_X^l$ this equation is solved by the bisection method for each species, O, S and Si. The depression of the melting point for each species is then obtained from equation (18). Finally, the melting temperature of the mixture, T_{m}, is calculated according to

$$T_{\mathrm{m}} = T_{\mathrm{m,Fe}} + \sum_i \Delta T_i, \tag{21}$$

where the sum is over O, S, and Si and $T_{\mathrm{m,Fe}}$ is given by equation (16). The liquid concentration evolves in time according to equation (2), which provides the value of $\bar{c}_X^l$ at each time point and the procedure is repeated.

The radial variation of thermal conductivity is parametrised by

$$k(r) = k_0 + k_1 r + k_2 r^2. \tag{22}$$

where k_0, k_1 and k_2 are coefficients that are obtained by fitting (22) to the data of Pozzo et al. (2013). This expression ignores the jump in k at the ICB (Pozzo et al., 2014), but this will cause only a slight change in the value of E_{k}.

The derivatives $\left(\frac{\partial \mu}{\partial c}\right)_{P,T}$ and $\left(\frac{\partial \mu}{\partial T}\right)_{P,c}$ of the chemical potential for O and Si are computed using the data of Alfè et al. (2002a) (see Gubbins et al. (2004) for details of the calculations). The quantity $\alpha_D = \rho D / \left(\frac{\partial \mu}{\partial c}\right)_{P,T}$, which arises in the entropy of molecular diffusion $E_{\rm a}$, also depends on the mass diffusion coefficients D for O and Si. Pozzo et al. (2013) found that D varies with depth for O, S, and Si, but this variation is unimportant for the calculations here because $E_{\rm a}$ is small and so we use constant D. The expansion coefficients α_c for O, S and Si are taken from Gubbins et al. (2004).

Symbol	Definition	Units	This Study		N14	P12
$T_{\rm a}$	Temperature	K				
$T_{\rm m}$	Melting temperature	K				
g	Gravity	m s^{-2}				
ψ	Gravitational potential	s^{-2}				
P	Pressure	Pa				
ρ	Density	kg m^{-3}				
$\mathbf{B}$	Magnetic field intensity	T				
σ	Electrical conductivity	S m^{-1}				
k	Thermal conductivity	W m^{-1}K^{-1}				
μ	Chemical potential	J mol^{-1}				
$\Delta\rho$	ICB density jump	g cc^{-1}	0.6, 0.8		0.8	0.8
$\frac{dT_{\rm o}}{dt}$	CMB cooling rate	K Gyr^{-1}				
h	Radiogenic heating by mass	W kg^{-1}				
$Q_{\rm cmb}$	Total CMB heat-flux	W				
$E_{\rm J}$	Ohmic heating	W K^{-1}				
C_p	Specific heat (constant pressure)	J kg^{-1} K^{-1}	715		840	715
L	Latent heat of freezing	MJ kg^{-1}	0.75		0.75	0.75
α_T	Thermal expansion coefficient	K^{-1} $\times 10^{-5}$	1.35		1.25	
μ_0	Permeability of free space	H m^{-1} $\times 10^{-7}$	4π		4π	4π
$r_{\rm o}$	Outer core radius	km	3480		3480	3480
$r_{\rm i}$	Inner core radius	km	1221		1220	1221
$M_{\rm c}$	Mass of core	kg $\times 10^{24}$	1.94		1.93	1.9477
$M_{\rm oc}$	Mass of outer core	kg $\times 10^{24}$	1.84		1.83	1.85
$g_{\rm i}$	ICB gravity	m s^{-2}	4.40		4.23	4.40
$\rho_{\rm i}$	ICB density	Mg m^{-3}	12.2		12.1	12.17
$\frac{\partial T_{\rm m}}{\partial P}\Big\vert_{r_{\rm i}}$		K Gpa^{-1}	9.01		9.36	9.0
			PREM	MG	MG	MG
$k_{\rm o}$	CMB thermal conductivity	W m^{-1} K^{-1}	107	99	130	100
$T_{\rm i}$	ICB temperature	K	5789	5497	5508	5500
$T_{\rm o}$	CMB temperature	K	4256	4046	4180	4039
$c^l_{\rm O}$	Liquid O Concentration		0.0256	0.0428	0.0409	0.0428
$c^l_{\rm S}$	Liquid S Concentration		0.0319	0.0263	-	-
$c^l_{\rm Si}$	Liquid Si Concentration		0.0279	0.0230	-	0.0461
$\frac{\partial T_{\rm a}}{\partial P}\Big\vert_{r_{\rm i}}$		K Gpa^{-1}	6.57	6.24	6.86	6.32

C_r		m K^{-1}	-10559	-9249	-10220	-9498

Table 1: Mathematical quantities used in the paper and, where relevant, the numerical values used in the calculations. Quantities in the third section are constant in time. Values in the fourth section are given for the present day; they are determined from the radial core structure. Quantities in the fifth section depend on the density jump at the inner core boundary (ICB). PREM refers to the model with ICB density jump $\Delta\rho = 0.6$ g cc^{-1} (Dziewonski and Anderson, 1981) and MG refers to the model with ICB density jump $\Delta\rho = 0.8$ g cc^{-1} (Masters and Gubbins, 2003).

2.2. Parameter Selection and Model setup

The expressions given in sections 2.1.1, 2.1.2 and 2.1.3 allow each of the integrals in equations (5) to be evaluated analytically. The calculations are straightforward but tedious; the results are given in the Appendix. Example profiles of ρ, $T_{\rm a}$, $T_{\rm m}$ and k are shown in Figure 2 and discussed in more detail in the following section.

Equations (5) are evolved backwards in time from the present-day for a period of 3.5 billion years using a timestep of 1 Myr, which is sufficient to resolve the rapid changes that arise around the time of inner core nucleation. The location of the ICB is found from the intersection of $T_{\rm a}$ and $T_{\rm m}$ at each timestep. Near the centre of the Earth $T_{\rm a}$ and $T_{\rm m}$ are almost parallel and so a small change in core temperature can change the predicted ICB radius from a few tens of km to a few metres; the inner core apparently "disappears". It is also possible for $T_{\rm a}$ to cross $T_{\rm m}$ twice, i.e. a transition from liquid to solid to liquid. Such spurious behaviour is avoided by ensuring that $\mathrm{d}T_{\rm a}/\mathrm{d}r$ obtained from equation (15) is shallower that the melting gradient in the innermost few km. This is easily achieved while fitting the coefficients in equation (15) to within the least squares errors. The procedure favours older inner core ages as it takes more time to raise the core adiabatic above $T_{\rm m}$ at all radii.

At the start of the calculation the coefficient $T_{\rm cen}$ that anchors the adiabatic temperature [equation (15)] is set such that $T_{\rm a}$ is equal to the melting temperature at the present ICB radius, $r_{\rm i} = 1221$ km. Subsequently, the CMB temperature is updated from the calculated value of $\mathrm{d}T_{\rm o}/\mathrm{d}t$ and this is used to calculate a new adiabat with a new value of $T_{\rm cen}$.

Liquid concentrations are evolved using equation (2). This is used to calculate a new melting curve that, together with the updated adiabat, define the new ICB radius. The core density (and hence gravity and pressure) may vary over time as the concentration changes, but this effect has been omitted as it was in previous studies (see Nimmo, 2014, for a review). We expect the effect to be minor because the concentration changes are very small (as demonstrated below), while the density decrease due to increasing light element concentration will be at least partially offset by a density increase as the core temperature falls. Also, we only account for changes in $k(r)$ due to the density jump and do not model the effect of time-varying concentration. The melting temperature, and hence the adiabatic temperature, do depend on temporal changes in light element concentration and so the coefficients $\tilde{E}$ and $\tilde{Q}$ in equations (5) also change in time.

As discussed above, the lack of observational constraints on the time evolution of $E_{\rm J}$ and $Q_{\rm cmb}$ mean they are effectively unknowns for the purpose of this study. To proceed we must fix one to determine the other. For the purpose of constructing minimum bound models it is clearly sufficient to take $Q_{\rm cmb}$ = constant or $E_{\rm J}$ = constant such that the minimum value of $E_{\rm J}$ in the past 3.5 Ga is ≥ 0.

Mantle convection simulations (e.g. Nakagawa and Tackley, 2013, 2014) and models of mantle thermal history (e.g. Jaupart et al., 2007) predict significant variations in $Q_{\rm cmb}$ with time and so we do not consider the case $Q_{\rm cmb}$ = constant. The simplest option, considered in section 4.1, is to set $E_{\rm J} = 0$, which gives the minimum allowable cooling rate (recall that $E_{\rm J}$ must be positive) and hence the oldest inner core and coolest ancient core temperature. However, this case produces an unrealistically sharp increase in $Q_{\rm cmb}$ at the time of inner core formation (Labrosse, 2003) and is therefore purely illustrative. Nimmo (2007) suggests fixing $E_{\rm J}$ = constant before inner core nucleation and $Q_{\rm cmb}$ = constant during inner core growth. This prescription has the advantage of producing the basic shape of $Q_{\rm cmb}(t)$ obtained in some mantle convection simulations (e.g. Nakagawa and Tackley, 2013, 2014) and is considered in section 4.2.

Parameter values used in this study are listed in column 4 of Table 1. Unless otherwise stated they are taken from the previous studies of Pozzo et al. (2012) and Pozzo et al. (2013). Parameter values used by Nimmo (2014) are listed in column 5 of Table 1. Parameter values used by Pozzo et al. (2012) are listed in column 6 of Table 1. The effects of different choices will be assessed in section 3. Parameters in the third section of Table 1 are taken to be constant in radius and time. Although α_T varies by a factor of two across the core (Gubbins et al., 2003), it only enters in the small terms associated with contraction and can safely be taken as constant without affecting the results; accounting for the variation of α_T requires a numerical solution that shows the contraction terms remain small (Gubbins et al., 2003). Parameters in the fourth section of Table 1 are derived from the radial profiles developed in the previous section. Parameters in the final section depend on the ICB density jump and core chemistry.

The most uncertain model input parameters are the ICB density jump $\Delta\rho$, the thermal conductivity, and the amount of radiogenic heat production h. Masters and Gubbins (2003) conclude that $\Delta\rho = 0.8 \pm 0.2$ gm cc^{-1}. Here we consider the two values $\Delta\rho = 0.6$ (denoted model PREM) and $\Delta\rho = 0.8$ gm cc^{-1} (denoted model MG) as described in section 2.1.3. Alfè et al. (2002b) do not distinguish between the behaviour of S and Si so for simplicity we assume they are present in equal (molar) amounts, i.e. 5% of both S and Si in the liquid for model PREM and 4% of both S and Si in the liquid for model MG. Solid concentrations are calculated from liquid concentrations as described in section 2.1.3 using the parameters listed in Table 2, which are taken from Alfè et al. (2002b) and Gubbins et al. (2013).

The thermal conductivity also depends on the nature and amount of impurity. Differences in recent estimates of $k_{\rm o} = k(r_{\rm o})$ = 80–110 W m^{-1} K^{-1} (de Koker et al., 2012; Pozzo et al., 2013; Gomi et al., 2013), and also in the radial variation of k, are in large part due to the

Symbol	Definition	Units	O	S	Si
$\bar{c}^s_X$ (PREM)	Solid concentration		0.0002	0.022	0.026
$\bar{c}^s_X$ (MG)	Solid concentration		0.0004	0.017	0.020
$\Delta\mu_0$	$\mu^l_0 - \mu^s_0$	eV/atom	-2.6	-0.25	-0.05
λ^s_X	Correction, solid		0.0	5.9	2.7
λ^l_X	Correction, liquid		3.25	6.15	3.6
α_c	Chemical expansion coefficient		1.1	0.64	0.87
D	Mass diffusivity	m^2 s$^{-1}\times10^{-8}$	1	0.5	0.5
α_D	Coefficient	kg m^{-3}s $\times10^{-12}$	0.70	0.81	0.75
$\left(\frac{\partial\mu}{\partial T}\right)_{P,c}$	CMB value	J mol^{-1} K^{-1} $\times10^{-4}$	-4.5	-	1.1
$\left(\frac{\partial\mu}{\partial T}\right)_{P,c}$	Centre of Earth value	J mol^{-1} K^{-1} $\times10^{-4}$	-2.3	-	1.9

Table 2: Parameters that define the model of core chemistry used in this study. Solid concentrations are given for the present-day.

use of different core compositions. Here we take a simple approach to account for these differences in k by using the two radial profiles of Pozzo et al. (2013) shown in Figure 2 and changing k_o. For model PREM, Pozzo et al. (2013) find $k_o = 107$ W m^{-1} K^{-1} so we take $k_0 = 100, 107$ and 115 W m^{-1} K^{-1} as representative of the variation. For model MG, Pozzo et al. (2013) find $k_o = 99$ W m^{-1} K^{-1} and so we take $k_o = 90, 99$ and 110 W m^{-1} K^{-1}.

The amount of radiogenic heat production in the core is still highly uncertain (Nimmo, 2007). To compare to previous studies that incorporate radiogenic heating we consider potassium (Nimmo et al., 2004). The amount of radiogenic heat production h is evolved backwards in time via the equation

$$h = h_0 2^{t/t_{1/2}}, \tag{23}$$

where $t_{1/2} = 1.248$ Gyr is the half-life of ^{40}K and h_0 is the present day heat production due to ^{40}K. The time variation produces a factor of 7 variation in h over 3.5 Ga. To compare with the results of Nimmo (2014) we consider $h_0 = 0$ and $h_0 = 300$ ppm. The latter is probably higher than is acceptable on geochemical grounds and represents an extreme scenario.

3. Comparison with previous models

Previous studies (Buffett et al., 1996; Labrosse et al., 1997; Nimmo, 2014) have adopted different parameter values and analytical expressions for radial core structure from those used here. To demonstrate the influence of the different choices we compare the model developed in section 2.1, here labelled POLY, to that used by Pozzo et al. (2012) (hereafter P12) and Nimmo (2014) (hereafter N14). The parameter values used in P12 and N14 are presented in Table 1. P12 only calculated the present-day core energy budget, but did so by numerically integrating equations (5) using the data for T_a, T_m, etc, obtained directly from seismic and mineralogical studies. Their present-day results serve as a benchmark with which to compare the POLY and N14 models. N14 calculated core thermal histories over the last 4.5 Gyr. To do so he followed Labrosse et al. (1997) by writing the density, adiabatic temperature, melting temperature and thermal conductivity as

$$
\begin{aligned}
\rho(r) &= \rho_{\rm cen} \exp^{-r^2/L^2}, && (24)\\
T_{\rm a}(r) &= T_{\rm cen} \exp^{-r^2/D^2}, && (25)\\
T_{\rm m}(r) &= T_{m0}(1 + t_{m1}P + t_{m2}P^2), && (26)\\
k(r) &= k(r_{\rm o}) \frac{1 - \frac{r^2}{D_K^2}}{1 - \frac{r_{\rm o}^2}{D_k^2}}, && (27)
\end{aligned}
$$

where $L \approx 7000$ km, $D \approx 6000$ km and D_k are lengths defined in Nimmo (2014). These profiles will be denoted N14ρ, N14$T_{\rm a}$, N14$T_{\rm m}$ and N14k. Note that Nimmo (2014) used $k = 130$ W m^{-1}K^{-1} independent of depth and so the same is done here. We first compare the radial profiles used in the POLY and N14 models to P12, who used the PREM density profile, the melting data of Alfè et al. (2002c) and equation (14) for $T_{\rm a}$ with $\gamma = 1.5$. We then compare models based on a published solution for the present-day energy budget before evolving this solution backwards in time using the POLY and N14 models.

Figure 2 compares the POLY and N14 radial profiles. The main difference between the density profiles is that N14ρ does not account for the ICB density jump. The theoretical adiabats and melting curves differ significantly at the top of the core. This difference between the melting curves is not important because $T_{\rm m}$ only enters the equations through $\mathrm{d}T_{\rm m}/\mathrm{d}r|_{r=r_{\rm i}}$. However, the difference in $T_{\rm a}$ at the top of the core is significant because $\partial T_{\rm a}/\partial r|_{r=r_{\rm o}}$ is needed to determine the adiabatic heat-flux and hence the condition of neutral stability. Using $k(r_{\rm o}) = 99$ W m^{-1} K^{-1} we find that $Q_{\rm k} = 14.8$ TW for the POLY $T_{\rm a}$ profile and $Q_{\rm k} = 11.5$ TW using the N14 $T_{\rm a}$ profile, a significant difference. The profiles of $T_{\rm m}$ and $T_{\rm a}$ are similar in the lower half of the core, but it should be noted that the gravitational energy and latent heat terms are very sensitive to small differences in $\mathrm{d}T_{\rm m}/\mathrm{d}P|_{r=r_{\rm i}}$ and $\partial T_{\rm a}/\partial P|_{r=r_{\rm i}}$. Values for these gradients and the parameter C_r [equation (3)] at the present day are given in Table 1 for the POLY, N14 and P12 models. The estimate of C_r using the POLY core structure is closest to the P12 value and differs by about 10% from the value obtained with the N14 core structure. This difference affects the terms $Q_{\rm L}$, $Q_{\rm PL}$, $Q_{\rm g}$ and the associated entropy terms.

Table 3 lists individual terms in the energy and entropy balance at the present-day for Case 5 of P12. This Case was chosen as it has also been reproduced by Nimmo (2014) (his Table 4) using a different code. P12 neglected pressure heating and the heat of reaction and this is also done here. In Table 3 the first part of each model name refers to the model of core structure that is used (P12, POLY and N14) while the last two characters in each name give the column number in Table 1 corresponding to the parameter values that are used.

Model POLYC4 calculates the melting behaviour as in section 2.1.3 and includes the effect of S and Si in the gravitational energy. Model POLYC6 is designed to reproduce the parameters adopted by P12. P12 set the ICB temperature to 5700 K; to mimic this we prescribe a time-independent $\Delta T_{\rm X}$ in equation (21) such than $T_{\rm m}(r_{\rm i}) = 5700$ K rather than calculating it by the method described in section 2.1.3. The N14 models also use a

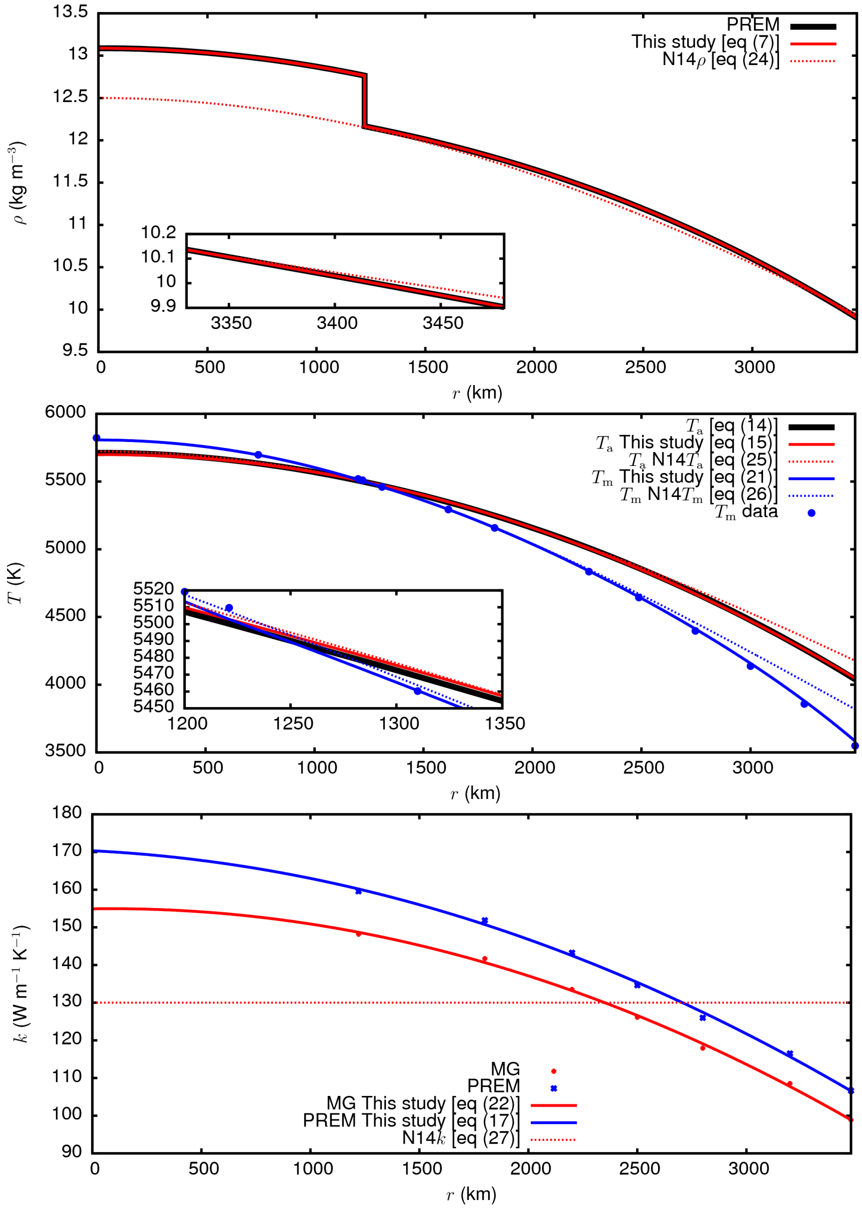

Figure 2: Top: radial variation of core density calculated from PREM (black line), Nimmo (2014) (red dashed line, equation (24)) and this study (red solid line, equation (7)). Inset shows a close-up of the profiles near the CMB. Middle: radial variation of the adiabatic temperature using equation (14) with g and ϕ calculated from PREM (black), this study (equation (15), red solid line) and Nimmo (2014) (equation (25), red dashed line). Also shown are the melting data of Alfè et al. (2002c) (blue points), the melting curve from this study (equation (21), blue solid line) and the melting curve from Nimmo (2014) (equation (26), blue dashed line). Melting point data were linearly interpolated from pressure to radius. Bottom: radial variation of thermal conductivity k using data from Pozzo et al. (2013) (points), this study (equation (22), solid lines) and Nimmo (2014) (equation (27), dashed line). PREM refers to the density jump $\Delta\rho = 0.6$ g cc^{-1} (Dziewonski and Anderson, 1981); MG refers to the density jump $\Delta\rho = 0.8$ g cc^{-1} (Masters and Gubbins, 2003).

Model	$Q_{\rm s}$	$Q_{\rm L}$	$Q_{\rm g}$	$Q_{\rm k}$	$E_{\rm s}$	$E_{\rm L}$	$E_{\rm g}$	$E_{\rm a}$	$E_{\rm k}$	$E_{\rm J}$	$\mathrm{d}T_{\rm o}/\mathrm{d}t$	IC age
P12C6	5.93	5.92	3.35	15.2	212	389	830	5.81	561	865	115	373
POLYC4	5.70	5.54	3.96	14.8	206	363	979	5.98	542	999	111	451
POLYC6	5.90	5.77	3.54	14.8	213	377	874	5.98	542	901	115	455
N14C5	6.01	5.78	3.41	14.9	181	333	816	0.0	451	877	102	500
N14C6	5.38	6.13	3.70	11.5	162	351	885	0.0	346	1047	108	490

Table 3: Comparison of different parameterisations of core structure with Case 5 of Pozzo et al. (2012). Individual terms are defined in the text. All energy terms are in TW; entropy terms are in MW K^{-1}; $\mathrm{d}T_{\rm o}/\mathrm{d}t$ in K Gyr^{-1}; inner core (IC) age in Myr. $Q_{\rm cmb} = 15.2$ TW in all models. Model P12C6 corresponds to the results of Pozzo et al. (2012) and uses the parameters in column 6 (C6) of Table 1. Model POLYC4 uses the POLY core structure developed in section 2.1 and the parameters listed in column 4 (C4) of Table 1. Model POLYC6 uses the POLY core structure and is set up to reproduce the values in column 6 (C6) of Table 1. Model N14C5 is calculated using equations (24)–(27) for the Nimmo (2014) core structure and values for quantities given in Nimmo (2014) and column 5 of Table 1. Model N14C6 is calculated using equations (24)–(27) for Nimmo (2014) core structure and parameter values adopted in column 6 of Table 1. Pressure heating and heat of reaction have been neglected. All cases use model MG for core chemistry.

time-independent melting point depression. For model POLYC6 and the N14 models it is assumed, as in P12, that only O contributes to the gravitational energy and that all the O partitions into the liquid on freezing.

Table 1 shows that there is good agreement between the P12C6, POLYC6 and N14C5 models. In particular, all terms in model POLYC6 are within ∼5% of the corresponding term for the P12C6 case. The POLYC4 model has more gravitational energy than model P12C6 because it accounts for contributions from S and Si; indeed, the contribution of O alone is 3.36 TW, very close to that of model P12. Model N14C5 is close to model P12C6 but uses different values of C_p and k and so predicts a slower present-day cooling rate. There is weaker agreement between N14C6 and the other models.

Figure 3 shows the POLY and N14 models in Table 3 evolved backwards in time with $Q_{\rm cmb}$ fixed during inner core growth and $E_{\rm J}$ fixed prior to inner core formation. This choice is made purely to illustrate the different model behaviour. Because the models are evolved backwards in time, the fixed value of $E_{\rm J}$ equals the value obtained at the first instant when there was no inner core. The difference in predicted inner core age for the POLY and N14 models is ∼50 Myr, which is about 10% of the ages that are obtained below. More importantly, model N14C5 predicts that a dynamo persists for the last 3.5 Ga while the other models predict that the dynamo fails around the time of inner core nucleation. Both POLY and N14 models predict an older inner core than P12C6 indicating that the assumption of a constant cooling rate, which was used by P12 to calculate the inner core age, is not borne out by the evolution models.

There are two reasons for the similar behaviour of models POLYC4 and POLYC6 in Figure 3. First, the $\Delta T_{\rm X}$ computed using equation (18) are only weakly depth-dependent, partly because liquid and solid concentrations do not change significantly over time and partly because the increase of $T_{\rm m,Fe}$ with pressure is mostly offset by a decrease in $\Delta S_{\rm Fe}$ with pressure. Second, S and Si contributions to the gravitational energy (and entropy) are

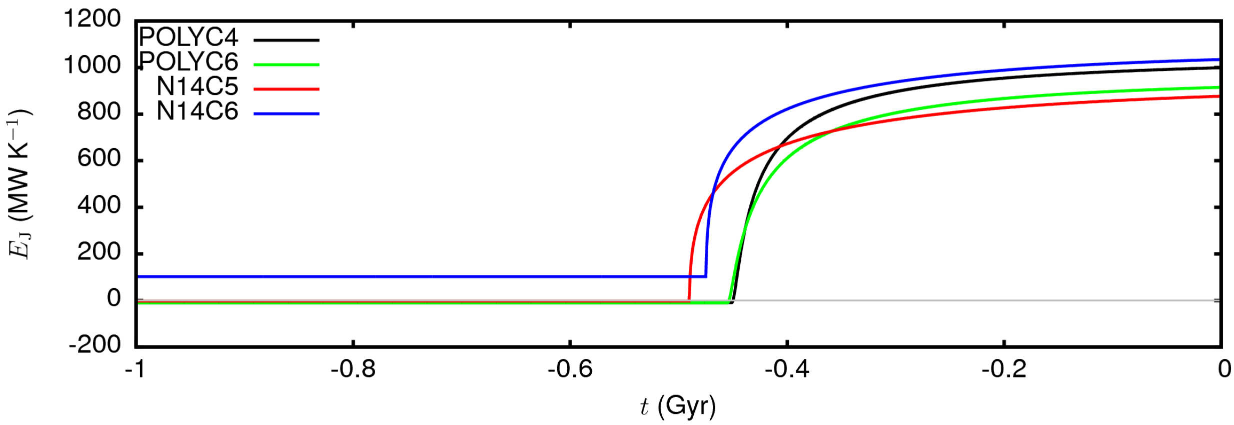

Figure 3: Power available to drive the dynamo E_J over time for the different models of core structure shown in Table 3. The present-day is at time $t = 0$.

at least an order of magnitude smaller than the contribution from O. An example of this behaviour is shown in section 4.2 below.

We note that considering just the present-day energetics of the core suggests that Case 5 would generate a magnetic field for the whole of Earth's history (Pozzo et al., 2012). However, Figure 3 shows that there is insufficient power available to the dynamo before inner core nucleation owing to the increase in conduction entropy with age. This example shows the importance of analysing the whole cooling history rather than just the present-day energy budget.

The heat of reaction and pressure heating were ignored in the calculations shown in Figure 3 and Table 3 in order to compare with previous results. These terms were found to be small in the present-day core energy budget (Gubbins et al., 2003, 2004). Table 4 shows how the inclusion of these terms affects the predicted inner core age and ancient core temperature for the calculations in Table 3. The heat of reaction E_h makes no difference to the results and can be safely ignored. Adding the pressure heating makes the inner core 25 Myr older than the calculations in Table 3 and decreases the ancient core temperature by 10 K. We regard this difference as small and ignore the pressure heating terms from now on. Table 4 also shows that changing the value of C_p from 715 J kg^{-1} K^{-1} (used in this study) to 840 J kg^{-1} K^{-1} (used by (Nimmo, 2014)) increases the predicted inner core age by 25 Myr and lowers the ancient core temperature by 175 K.

4. Minimum entropy core cooling models

We now present models of marginal dynamo evolution, i.e. models with the minimum E_J such that $E_J \geq 0$ for all time. Unless stated, results use model MG for core chemistry. Results for models with different values of $\Delta\rho$, h and $k(r_o)$ are summarised in Figure 7. Parameter values are listed in column 4 of Table 1.

C_p	E_h (W K^{-1})	$Q_\mathrm{P} + Q_\mathrm{PL}$ (TW)	IC age (Myr)	T_an (K)
715	0	0	451	5104
715	13	0	451	5104
715	0	1.06	477	4994
840	0	0	477	4949
840	0	1.00	510	4938

Table 4: Effect of changing the specific heat capacity C_p, heat of reaction E_h and pressure heating $Q_\mathrm{P}+Q_\mathrm{PL}$ on predicted inner core age and core temperature at 3.5 Ga (T_an) for the Case shown in Figure 3 and Table 3. The POLY core structure developed in section 2.1 has been used.

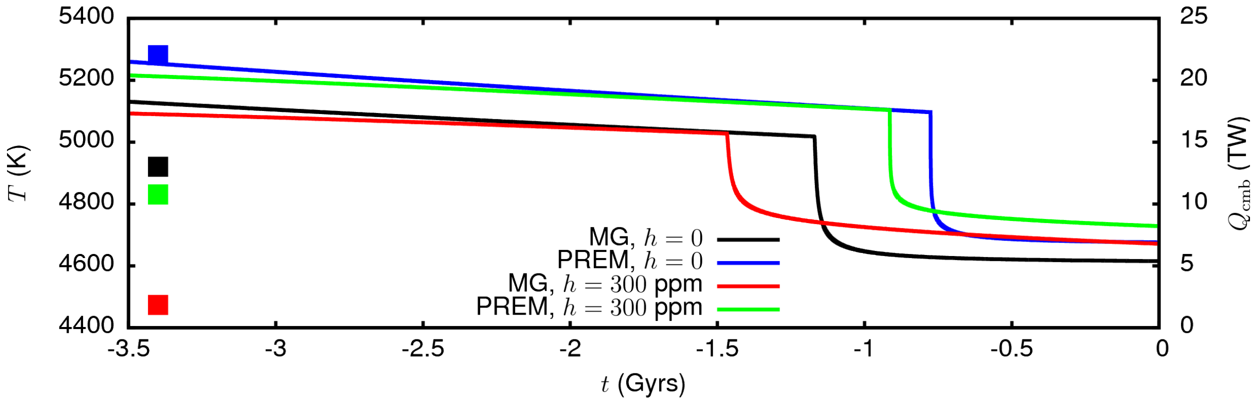

Figure 4: Marginal dynamo evolution with $E_\mathrm{J} = 0$ fixed in time. $Q_\mathrm{cmb} < Q_\mathrm{k}$ during inner core solidification in these models. CMB heat-flux Q_cmb (solid lines) is plotted on the right ordinate; temperature at the top of the core at 3.5 Ga (squares) is plotted on the left ordinate. The present-day is at $t = 0$. Parameters are given in column 4 of Table 1. See text for details.

4.1. Fixed Dynamo Power

Figure 4 shows the evolution of Q_cmb when E_J is set to zero for all time. The unrealistic jump in Q_cmb following inner core formation is clear. In these models $Q_\mathrm{cmb} < Q_\mathrm{k}$ following inner core formation and so a stable region may be present at the top of the core. The larger density jump in model MG increases the gravitational energy, allowing the entropy budget to be balanced with a lower cooling rate than for model PREM. Cooling histories with the MG core model therefore predict an older inner core and lower ancient core temperature than those with the PREM core model. Adding radiogenic heating also slows down the cooling rate. The present-day CMB heat-flux required to sustain a marginal dynamo is in the range $5.5 - 8.5$ TW; at 3.5 Ga, $Q_\mathrm{cmb} = 15 - 20$ TW. Predicted inner core ages range between 0.75 and 1.5 Ga. All models yield an ancient core temperature greater than 4400 K, which far exceeds estimates of 4150±150 K for the lower mantle solidus (Andrault et al., 2011)

Increasing E_J to ensure the core remains superadiabatic for the last 3.5 Ga strongly increases the power requirements. For the MG density jump and no radiogenic heating, $E_\mathrm{J} = 918$ MW K^{-1} is required to ensure $Q_\mathrm{cmb} > Q_\mathrm{k}$. The model predicts an inner core age of only 440 Myr and a very high CMB temperature of 7448 at 3.5 Ga.

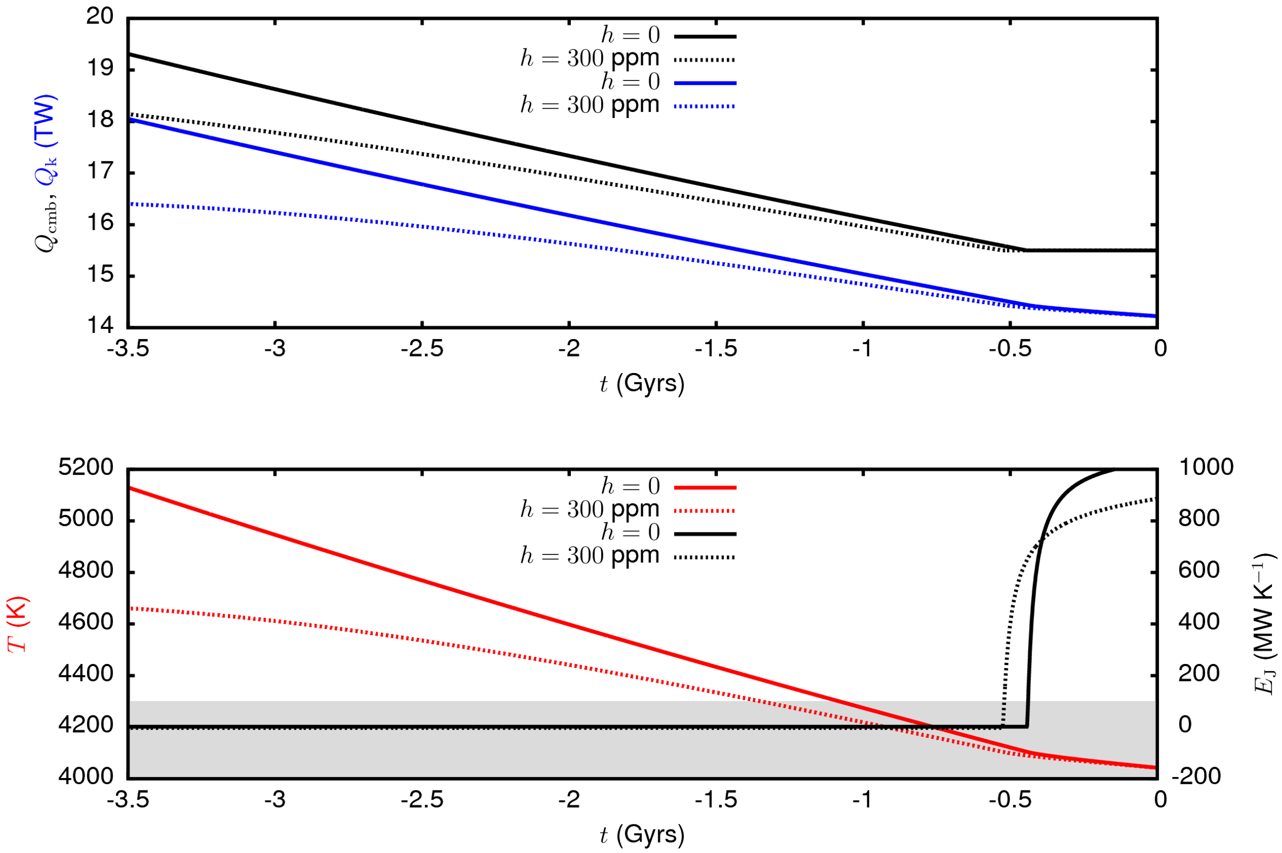

Figure 5: Marginal dynamo evolution with $Q_{\rm cmb}$ fixed during inner core growth and $E_{\rm J}$ fixed prior to inner core formation. Two models are shown: $h = 0$ assumes no radiogenic heating; $h = 300$ ppm assumes 300 ppm of ^{40}K in the core at the present-day. Top panel: CMB heat-flux $Q_{\rm cmb}$ and heat conducted down the adiabatic gradient $Q_{\rm k}$. Bottom panel: temperature at the top of the core is shown on the left ordinate; $E_{\rm J}$ is shown on the right ordinate. The grey shaded region shows the range of lower mantle solidus temperatures estimated by Andrault et al. (2011). The present-day is at $t = 0$. Parameters are given in Table 1. See text for details.

4.2. Fixed CMB heat-flux

Figure 5 shows marginal dynamo evolution when $Q_{\rm cmb}$ is fixed during inner core growth and $E_{\rm J}$ is fixed prior to inner core formation. $E_{\rm J}$ increases rapidly during inner core growth because of latent heat and gravitational energy sources. $Q_{\rm cmb}$ always exceeds the adiabatic heat-flux $Q_{\rm k}$, as it must for $E_{\rm J}$ to remain positive in this case. At the present-day, this cooling history yields a high CMB heat-flux of 15.5 TW. The inner core age is 444 Myr, while the ancient core temperature of 5130 K is very high. In this model the core temperature exceeds current estimates of the lower mantle solidus until around 1 Ga, suggesting that the lower mantle would be at least partially molten for most of Earth's history.

Figure 5 also shows the model with minimum $E_{\rm J}$ that contains an additional 300 ppm of potassium at the present-day. As is well known (e.g. Nimmo et al., 2004), the addition of radiogenic heating slows core cooling while making only a small change to the entropy budget. Nevertheless, the model still predicts a young inner core age of 526 Myr and a high

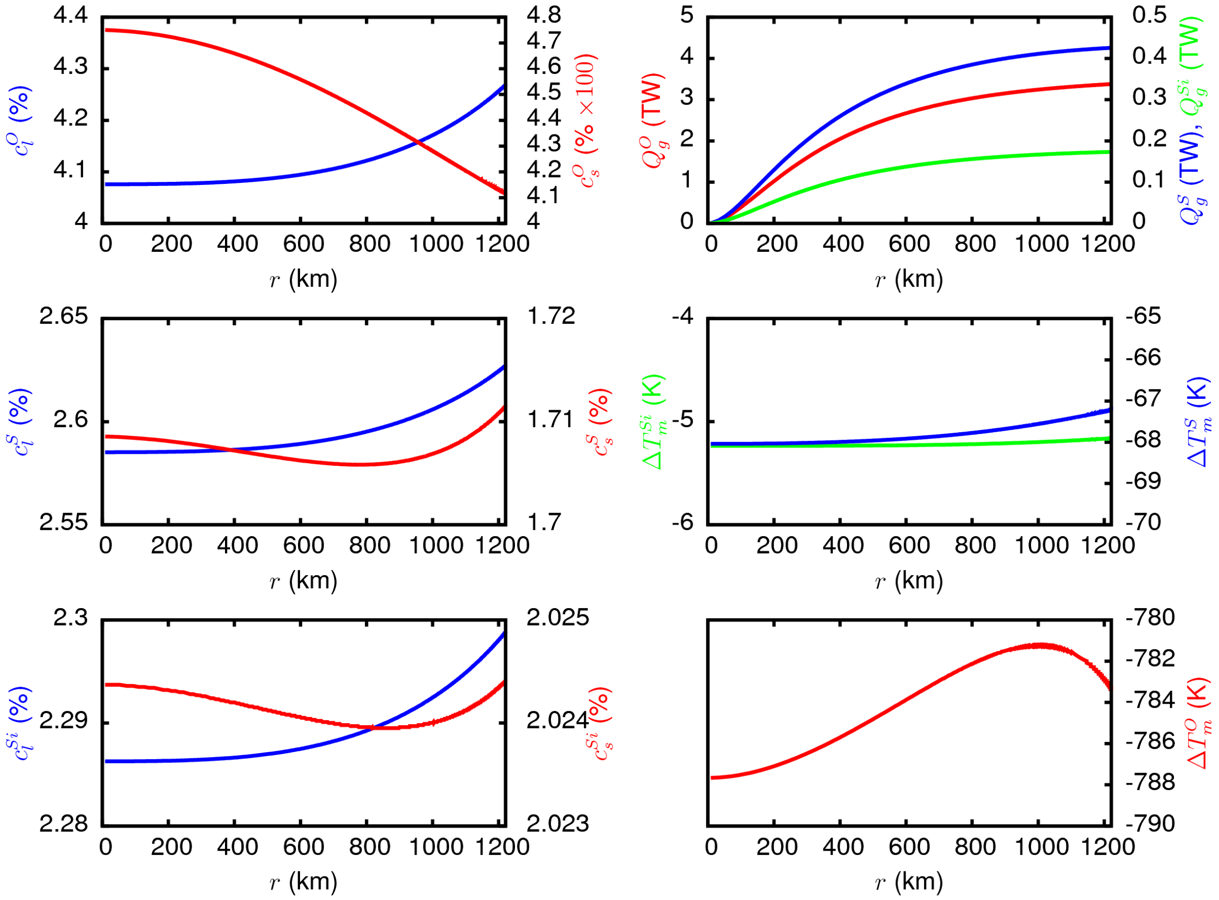

Figure 6: Effect of time-varying light element concentrations in the MG model of core chemistry. All quantities are plotted as functions of the inner core boundary radius, r. Top left: O concentration in the liquid (blue) and solid (red); middle left: S concentration in the liquid (blue) and solid (red); bottom left: Si concentration in the liquid (blue) and solid (red). All concentrations are given as mass fractions. Top right: contributions to the gravitational energy $Q_{\rm g}$ from O (red), S (blue) and Si (green); middle right: depression of the melting point due to Si (green) and S (blue); bottom right: depression of the melting point due to O (red). Note the different limits on the axes.

early core temperature of 4660 K. In this model the core temperature drops below the upper estimate of 4300 K for the lower mantle solidus at 1350 Ma.

Figure 6 shows the partitioning and melting behaviour. The results are plotted against inner core radius rather than time and hence apply to all models with the MG density jump. Each of the light element concentrations vary by less than 5% of their present-day values over the timescale of inner core growth. Almost all the O partitions into the liquid on freezing, Si partitions almost equally and about 65% of the S goes into the liquid. The gravitational energy is therefore dominated by the contribution from O, while the Si contribution is much less than that of S. The melting point depression varies little with inner core radius because the concentration changes are small. Again, O dominates the melting point depression, while the contribution from Si is negligible. The presence of S depresses the melting point by almost 70 K; given that the core cools by, say, 100 K over 1 Ga this contribution is significant.

Figure 7 plots inner core age against present-day CMB heat flow, $Q_{\rm Pres}$, for a variety of marginal core histories with $Q_{\rm cmb}$ fixed during inner core growth and $E_{\rm J}$ fixed prior to inner core formation. Adding radiogenic heating, all other things being equal, increases the inner core age and slightly changes $Q_{\rm Pres}$. Increasing the thermal conductivity at the top of the core substantially decreases the inner core age and increases $Q_{\rm Pres}$: for model MG, $h = 0$ and $k_0 = 90$ W m^{-1} K^{-1} the inner core age is 480 Myr and $Q_{\rm Pres} = 14.4$ TW while the same model with $k_0 = 110$ W m^{-1} K^{-1} gives an age of 405 Myr and $Q_{\rm Pres} = 17.0$ TW. The PREM density jump gives a younger inner core and higher $Q_{\rm Pres}$ than the MG density jump.

Figure 7 also shows the core temperature at 3.5 Ga, $T_{\rm an}$, plotted against the age t_s (before present) when the core temperature fell below 4300 K, which is the highest value of the lower mantle solidus temperature using the error estimates of Andrault et al. (2011). Adding radiogenic heating increases t_s and decreases $T_{\rm an}$ while higher values of k_0 decrease t_s and increase $T_{\rm an}$. The PREM density jump yields much lower values of t_s and slightly higher values of $T_{\rm an}$ than the MG density jump. The message from this Figure is that all cooling histories yield an inner core age younger than 600 Myr, and core temperature at 3.5 Ga that far exceeds present estimates of the lower mantle solidus temperature. All models suggest the lower mantle was at least partially molten until at least the last 1.5 Ga. Sustaining a marginal dynamo over the last 3.5 Ga with a superadiabatic core requires the present-day CMB heat flow to exceed $\sim$14 TW.

5. Discussion and conclusions

The cooling history of Earth's core has been investigated using a 4-component (iron plus oxygen, sulphur and silicon) analytical thermodynamic model. The study was motivated by recent upward revision of the thermal conductivity of liquid iron mixtures (de Koker et al., 2012; Pozzo et al., 2013; Gomi et al., 2013), which was previously found to drastically reduce the power available to the geodynamo at the present-day (Pozzo et al., 2012). Because the geomagnetic field is known to have survived for at least the last 3.45 Ga (Tarduno et al., 2010), core cooling histories that constrain the thermodynamic conditions under which the geodynamo can persist are crucial for obtaining a coherent picture of long-term geomagnetic field evolution.

There are three novel aspects to the present thermodynamic model. First, it uses a polynomial representation of radial core structure (density, temperature, etc) that gives a good fit to present-day profiles derived from seismological and mineralogical data. The analytical expressions derived from these profiles are shown to produce results for the core energy and entropy budgets in close agreement with previous studies that numerically integrated the raw data. Second, the model incorporates a pressure-dependent melting point depression that also depends on the time evolution of O, S, and Si concentrations in the solid and liquid. Labrosse (2014) has investigated partitioning of O and S and similar results are obtained here. The variation of Si in the solid follows that of S, falling at first before increasing, further supporting the view (Labrosse, 2014) that the inner core is compositionally stably

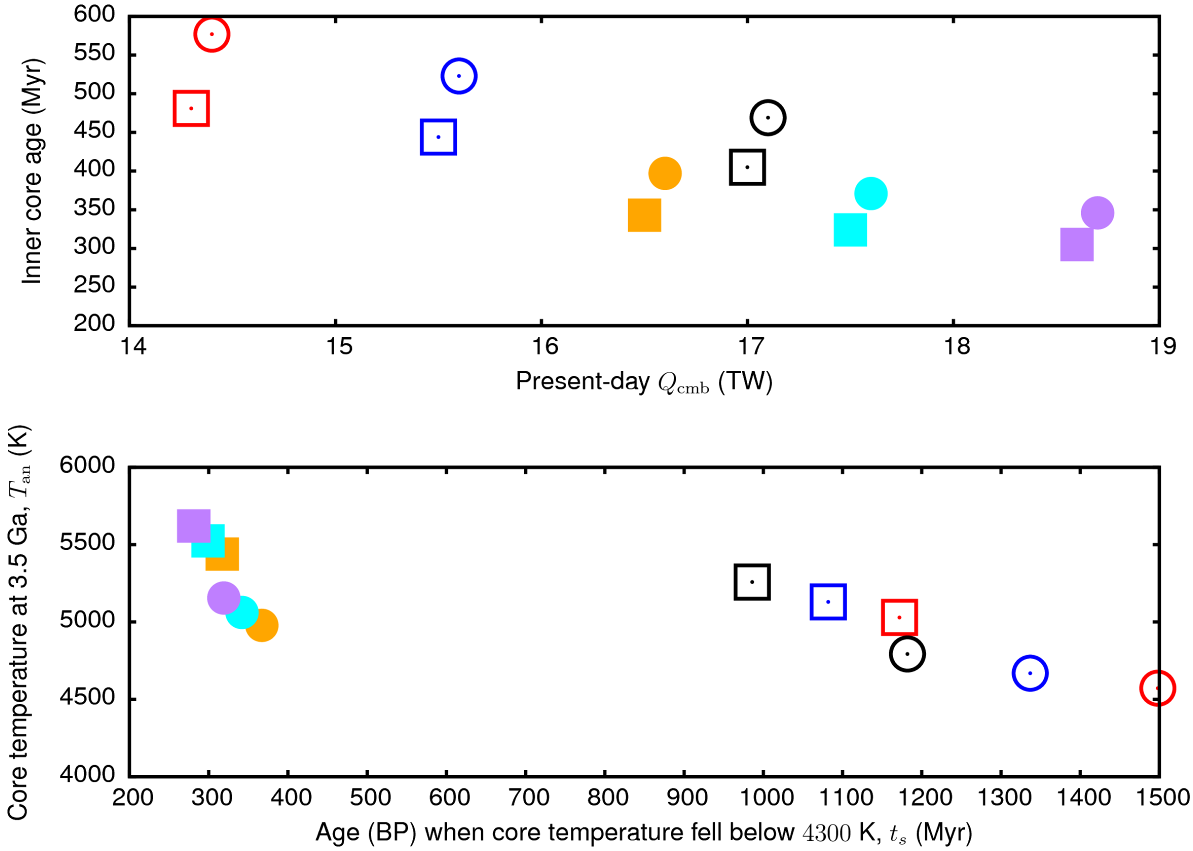

Figure 7: Phase diagram of present-day $Q_{\rm cmb}$ plotted against inner core age (top) and ancient core temperature $T_{\rm an}$ plotted against the age t_s where the core temperature fell below 4300 K (bottom). All cooling histories correspond to marginal dynamo evolution and have $Q_{\rm cmb}$ fixed during inner core growth and $E_{\rm J}$ fixed prior to inner core formation. Solid symbols denote cooling histories with the PREM core model; open symbols use the MG core model. Squares denote histories with $h = 0$; circles denote histories with 300 ppm of ^{40}K at the present-day. Colours show different values of the thermal conductivity at the top of the core: for model MG, k_0 =90 (red), 99 (blue) and 110 (black); for model PREM, k_0 =100 (orange), 107 (cyan) and 115 (purple).

stratified rather than unstable (Gubbins et al., 2013). Third, the gravitational energy released by each light element is calculated. The contribution from O is dominant because almost all the O partitions into the liquid on freezing in the model of core chemistry adopted in this study.

The main results of the paper are summarised in Figure 7. All cooling histories have a young inner core, less than 600 Myr old, and core temperatures at 3.5 Ga between 4500 and 5500 K. These results are broadly consistent with those obtained by Nimmo (2014) who found an inner core age of $\leq$ 700 Myrs and early core temperatures above 5000 K. Accounting for uncertainties in the input parameters such as the specific heat and the omission of pressure heating and heat of reaction (section 3) can increase the inner core age by $\sim$50 Myr and decrease the ancient core temperature by $\sim$70 K. However, even accounting for these uncertainties gives an inner core age much younger than the 1 Gyr obtained with old (low) values of the thermal conductivity (Labrosse et al., 2001) and a core primordial core temperature that far exceeds present estimates of 4150 ± 150 K for the lower mantle solidus (e.g. Andrault et al., 2011). The core temperature in these cooling histories exceeded the lower mantle solidus for most of the last 3.5 Ga, dropping below it in the last 0.3–1.5 Myr.

It may be possible to obtain slower core cooling rates than those predicted in this study, but the options are not particularly appealing. One option is to increase the amount of radiogenic potassium in the core; however, the 300 ppm used in this study is on the upper end of present estimates (Nimmo, 2014) and some studies argue that there is no radioactive heating in the core at all (Davies, 2007). Another possibility is that the uppermost core is strongly subadiabatic (see Figure 4). Pozzo et al. (2012) and Gomi et al. (2013) suggest that this scenario will involve a stable layer at the top of the core that is hundreds of kilometres thick, which is likely to be inconsistent with geomagnetic secular variation (Gubbins, 2007; Buffett, 2014). Moreover, the cooling histories in Figure 4 have early core temperatures in excess of 4300 K even though they have the Ohmic heating $E_{\rm J} = 0$ for all time. A third option is that the density jump at the inner core boundary (ICB) is higher than the $\Delta\rho = 0.6, 0.8$ g cc^{-1} used in this work. Masters and Gubbins (2003) find $\Delta\rho = 0.8 \pm 0.2$ g cc^{-1}. However, if the trend between cooling histories with $\Delta\rho = 0.6$ and 0.8 g cc^{-1} in Figure 7 persists up to $\Delta\rho = 1$ g cc^{-1} the predicted inner core age will still be significantly less than 1 Gyr and the ancient core temperature will exceed 4300 K. A fourth option is to use different models of core chemistry. We have assumed equal amounts of S and Si for each density jump, but other options are possible. Moreover, other elements such as H (Nomura et al., 2014) could be present in the core. The formalism presented above for computing partition coefficients and the melting point depression can be applied to any core chemistry model where the light elements behave independently. At present, testing this option require more data from mineral physics. Finally, it should be noted that there is still uncertainty in the adiabatic temperature and the melting curve for pure iron, which affect the calculated inner core growth rate and melting point depression. One set of temperature profiles have been adopted for this study. Future work will consider the effect of other choices.

The models in this study correspond to a state of marginal dynamo evolution, i.e. they yield the minimum $E_{\rm J}$ such that $E_{\rm J} \geq 0$ for all time. In the Earth's core $E_{\rm J}$ certainly exceeds that for a marginal dynamo at the present-day and probably has done for the last

3.5 Ga (e.g. Roberts et al., 2003; Gubbins et al., 2003). Higher values of E_J require higher core cooling rates to balance the entropy budget, resulting in higher core-mantle boundary (CMB) heat flows, a younger inner core age and a hotter primordial core than the estimates given here. Putting $E_J \sim 10^8$ W K^{-1} (Roberts et al., 2003) will easily offset any decrease in cooling rate that could be found from the options suggested about. It therefore seems inevitable that future models of coupled core-mantle evolution must contend with high CMB heat flows, high core temperatures, long-lived partial melting at the base of the mantle, and possibly stratification at the top of the core.

A high present-day CMB heat flow of > 14 TW is needed to maintain the geodynamo unless the top of the core in subadiabatic in which case 6–9 TW ensures a marginal dynamo. At 3.5 Ga CMB heat flows of $\sim$15 TW are needed to maintain a marginal dynamo. We also note that cooling histories with the PREM ICB density jump require present-day CMB in the range 16–18 TW depending on the thermal conductivity. Pozzo et al. (2013) find $k = 99$ W m^{-1} K^{-1} at the CMB for the PREM ICB density jump; if this value is an under-estimate, the CMB heat flow required to maintain an adiabatic core will exceed independent estimates of 7–17 TW for CMB heat flow (Lay et al., 2009; Nimmo, 2014).

The high primordial core temperatures are consistent with models of an ancient magma ocean at the base of the mantle. Labrosse et al. (2007) and Ziegler and Stegman (2013) both propose models that have a molten lowermost mantle at the present-day, although the thickness of their molten layers are rather different. However, the possibility that such a magma ocean would thermally insulate the core (Labrosse et al., 2007) raises the question of whether the core can cool rapidly enough beneath this thermal blanket to sustain the magnetic field at early times. Chemical exchange may also take place between the core and magma ocean. If this occurs then the direction of exchange will likely be crucial for early core dynamics; emplacing light material at the top of the core would lead to chemical stratification unless existing convection could mix the heterogeneity. Modelling the simultaneous evolution of core and magma ocean should shed light on the viability of an early core dynamo.

Acknowledgements

C.D. is supported by Natural Environment Research Council fellowships NE/H01571X/1 and NE/L011328/1 and a fellowship from the Green Foundation at IGPP, Scripps Institution of Oceanography. The author thanks Prof. Dario Alfè for providing data and Prof. Francis Nimmo for many valuable discussions. The use of a polynomial representation of core structure was motivated by stimulating discussions with John Hernlund, Stéphane Labrosse and David Gubbins at the Onsen II meeting in Tokyo, Japan (October 2013). The constructive and detailed comments of Stéphane Labrosse and an anonymous reviewer are gratefully acknowledged.

Appendix

This Appendix contains analytical expressions for the integrals in equations (5) derived from the polynomial expressions for radial core structure given in section 2. The integrals in the entropy terms $E_{\rm a}$, $E_{\rm k}$ and $E_{\rm r}$ are of the form $X(r)/T_{\rm a}(r)$ and hence the analytical expressions are very long. We present the results for $E_{\rm r}$ below; the derivations of $E_{\rm a}$ and$E_{\rm k}$ are similar. In practice it is just as easy to numerically integral $E_{\rm a}$, $E_{\rm k}$ and $E_{\rm r}$. Both approaches have been attempted here and the results are very similar.

Secular Cooling

The secular cooling term is given by

$$Q_{\rm s} = -\frac{C_p}{T_{\rm o}}\int \rho(r)T_{\rm a}(r){\rm d}V\frac{{\rm d}T_{\rm o}}{{\rm d}t} = -4\pi\frac{C_p}{T_{\rm o}}\int_0^{r_{\rm o}} \rho(r)T_{\rm a}(r)r^2{\rm d}r\frac{{\rm d}T_{\rm o}}{{\rm d}t}.$$

Using equations (7) and (15) the integral can be written as

$$\int \rho(r)T_{\rm a}(r){\rm d}V = 4\pi\left[S_{\rm o}(r_{\rm o}) - S_{\rm o}(r_{\rm i}) + S_{\rm i}(r_{\rm i})\right],$$

where

$$S_{\rm o}(r) = \frac{s_1^{\rm o}}{3}r^3 + \frac{s_2^{\rm o}}{4}r^4 + \frac{s_3^{\rm o}}{5}r^5 + \frac{s_4^{\rm o}}{6}r^6 + \frac{s_5^{\rm o}}{7}r^7 + \frac{s_6^{\rm o}}{8}r^8 + \frac{s_7^{\rm o}}{9}r^9,$$

and

$$S_{\rm i}(r) = \frac{s_1^{\rm i}}{3}r^3 + \frac{s_2^{\rm i}}{4}r^4 + \frac{s_3^{\rm i}}{5}r^5 + \frac{s_4^{\rm i}}{6}r^6 + \frac{s_5^{\rm i}}{7}r^7 + \frac{s_6^{\rm i}}{8}r^8.$$

Here

$$\begin{aligned}
s_1^{\rm o} &= \rho_0^{\rm oc}T_{\rm cen},\\
s_2^{\rm o} &= \rho_0^{\rm oc}T_{\rm cen}t_1 + \rho_1^{\rm oc}T_{\rm cen},\\
s_3^{\rm o} &= \rho_2^{\rm oc}T_{\rm cen} + \rho_1^{\rm oc}T_{\rm cen}t_1 + \rho_0^{\rm oc}T_{\rm cen}t_2,\\
s_4^{\rm o} &= \rho_3^{\rm oc}T_{\rm cen} + \rho_2^{\rm oc}T_{\rm cen}t_1 + \rho_1^{\rm oc}T_{\rm cen}t_2 + \rho_0^{\rm oc}T_{\rm cen}t_3,\\
s_5^{\rm o} &= \rho_3^{\rm oc}T_{\rm cen}t_1 + \rho_2^{\rm oc}T_{\rm cen}t_2 + \rho_1^{\rm oc}T_{\rm cen}t_3,\\
s_6^{\rm o} &= \rho_3^{\rm oc}T_{\rm cen}t_2 + \rho_2^{\rm oc}T_{\rm cen}t_3,\\
s_7^{\rm o} &= \rho_3^{\rm oc}T_{\rm cen}t_3,
\end{aligned}$$

and

$$\begin{aligned}
s_1^{\rm i} &= \rho_0^{\rm ic}T_{\rm cen},\\
s_2^{\rm i} &= \rho_0^{\rm ic}T_{\rm cen}t_1,\\
s_3^{\rm i} &= \rho_2^{\rm ic}T_{\rm cen} + \rho_0^{\rm ic}T_{\rm cen}t_2,\\
s_4^{\rm i} &= \rho_2^{\rm ic}T_{\rm cen}t_1 + \rho_0^{\rm ic}T_{\rm cen}t_3,\\
s_5^{\rm i} &= \rho_2^{\rm ic}T_{\rm cen}t_2,\\
s_6^{\rm i} &= \rho_2^{\rm oc}T_{\rm cen}t_3.
\end{aligned}$$

Gravitational energy

Gubbins et al. (2004) shows that

$$Q_{\mathrm{g}} = \alpha_c \frac{Dc_X^l}{Dt} \int \rho(r)\psi(r)\mathrm{d}V = \alpha_c \frac{Dc_X^l}{Dt} \left[4\pi \int_{r_{\mathrm{i}}}^{r_{\mathrm{o}}} \rho(r)\psi(r) r^2 \mathrm{d}r - M_{\mathrm{oc}}\psi(r_{\mathrm{i}}) \right].$$

Using equations (7) and (12) we find

$$\int \rho(r)\psi(r)\mathrm{d}V_{\mathrm{oc}} = 16\pi^2 G \left[G_c(r_{\mathrm{o}}) - G_c(r_{\mathrm{i}}) + G_b(r_{\mathrm{o}}) - G_b(r_{\mathrm{i}}) \right] \tag{28}$$

where

$$G_c(r) = g_1^{\mathrm{o}} r^5 + g_2^{\mathrm{o}} r^6 + g_3^{\mathrm{o}} r^7 + g_4^{\mathrm{o}} r^8 + g_5^{\mathrm{o}} r^9 + g_6^{\mathrm{o}} r^{10} + g_7^{\mathrm{o}} r^{11} \tag{29}$$

and

$$G_b(r) = \psi(r_{\mathrm{o}}) \left(\frac{\rho_0^{\mathrm{oc}}}{3} r^3 + \frac{\rho_1^{\mathrm{oc}}}{4} r^4 + \frac{\rho_2^{\mathrm{oc}}}{5} r^5 + \frac{\rho_3^{\mathrm{oc}}}{6} r^6 \right) \tag{30}$$

where

$$\begin{aligned}
g_1^{\mathrm{o}} &= {\rho_0^{\mathrm{oc}}}^2/30, \\
g_2^{\mathrm{o}} &= \rho_0^{\mathrm{oc}} \rho_1^{\mathrm{oc}}/24, \\
g_3^{\mathrm{o}} &= {\rho_1^{\mathrm{oc}}}^2/84 + \rho_0^{\mathrm{oc}} \rho_2^{\mathrm{oc}} 13/420, \\
g_4^{\mathrm{o}} &= \rho_1^{\mathrm{oc}} \rho_2^{\mathrm{oc}}/ + \rho_0^{\mathrm{oc}} \rho_3^{\mathrm{oc}}/40, \\
g_5^{\mathrm{o}} &= {\rho_2^{\mathrm{oc}}}^2/180 + 7\rho_1^{\mathrm{oc}} \rho_3^{\mathrm{oc}}/540, \\
g_6^{\mathrm{o}} &= \rho_2^{\mathrm{oc}} \rho_3^{\mathrm{oc}}/120, \\
g_7^{\mathrm{o}} &= {\rho_3^{\mathrm{oc}}}^2/330.
\end{aligned}$$

Pressure Heating

The density differential can be written in terms of concentration, temperature and pressure:

$$\mathrm{d}\rho = \left(\frac{\partial \rho}{\partial c} \right)_{P,T} \mathrm{d}c + \left(\frac{\partial \rho}{\partial T} \right)_{P,c} \mathrm{d}T + \left(\frac{\partial \rho}{\partial P} \right)_{c,T} \mathrm{d}P.$$

We follow Gubbins et al. (1979) and use a simplified implementation of the pressure heating Q_{P} that neglects the thermal and pressure effects on density so that

$$\frac{D\rho}{Dt} = \rho \alpha_c \frac{Dc}{Dt}.$$

These approximations are justified by the smallness of Q_{P} and its associated entropy E_{P}. Moreover, the results obtained here give good agreement with those obtained by Gubbins et al. (2003), who performed a more complex calculation.

Differentiating the hydrostatic equation (13) gives

$$
\begin{aligned}
\frac{DP}{Dt} &= -\int_{r_\mathrm{o}}^{r} \frac{D\rho}{Dt}\frac{4\pi G}{r^2}\left[\int_0^r \rho r'^2 \mathrm{d}r'\right]\mathrm{d}r - \int_{r_\mathrm{o}}^{r} \frac{4\pi G\rho}{r^2}\left[\int_0^r \frac{D\rho}{Dt} r'^2 \mathrm{d}r'\right]\mathrm{d}r + \frac{DP}{Dt}(r_\mathrm{o}),\\
&= 8\pi G\alpha_c \frac{Dc}{Dt}\int_{r_\mathrm{o}}^{r} \frac{\rho}{r^2}\left[\int_0^r \rho r'^2 \mathrm{d}r'\right]\mathrm{d}r + \frac{DP}{Dt}(r_\mathrm{o}).
\end{aligned}
$$

The integral can be evaluated using equation (7) using the procedure to calculate the mass of the core [equation 9].

Radiogenic Heating

The entropy due to radiogenic heating depends on the integral

$$
\int \frac{\rho(r)}{T_\mathrm{a}(r)}\mathrm{d}V = 4\pi\int_0^{r_\mathrm{o}} \frac{\rho(r)}{T_\mathrm{a}(r)} r^2 \mathrm{d}r.
$$

This integral can be evaluated by long division and then partial fractions on the remainder. The result is

$$
\int \frac{\rho}{T_\mathrm{a}}\mathrm{d}V = 4\pi\left[\frac{A_3}{3}r_\mathrm{o} + \frac{B_3}{2t_3}r_\mathrm{o}^2 + \frac{C_3}{t_3}r_\mathrm{o} + X\log(r_\mathrm{o} - R_1) + Y\log(r_\mathrm{o} - R_2) + Z\log(r_\mathrm{o} - R_3)\right].
$$

where

$$
A = \frac{\rho_3^{\mathrm{oc}}}{t_3}; B_i = (\rho_i - At_i); C_i = B_i - -\frac{B_3}{t_3}t_i; D_i = C_i - \frac{C_3}{t_3}t_i.
$$

Here the index i runs from 0 to 2. The quantities X, Y and Z are given by

$$
\begin{aligned}
Z &= \left[D_2 - D_3(R_3 + R_2) - (R_1 - R_2) - (R_1 - R_2)\left(\frac{D_1 + D_3R_2R_3}{(R_2R_3 - R_1R_3)}\right)\right] \times\\
&\quad \left[(R_1 - R_3) + (R_2 - R_1)\left(\frac{R_2R_3 - R_1R_2}{R_2R_3 - R1R_3}\right)\right]^{-1},\\
Y &= \frac{D_1 + D_3R_2R_3 - C(R_2R_3 - R_1R_2)}{(R_2R_3 - R_1R_3)},\\
X &= D_3 - B - C.
\end{aligned}
$$

Here R_1, R_2 and R_3 are the three roots of $T_\mathrm{a}(r)$.

References

Alfè, D., Gillan, M., Price, G., 2002a. Ab initio chemical potentials of solid and liquid solutions and the chemistry of the Earth's core. J. Chem. Res. 116, 7127–7136.

Alfè, D., Gillan, M., Price, G., 2002b. Composition and temperature of the Earth's core constrained by combining ab initio calculations and seismic data. Earth Planet. Sci. Lett. 195, 91–98.

Alfè, D., Gillan, M. J., Price, G. D., 2007. Temperature and composition of the Earth's core. Contemp. Phys. 48, 63–80.

Alfè, D., Price, G., Gillan, M., 2002c. Iron under Earth's core conditions: Liquid-state thermodynamics and high-pressure melting curve from ab initio calculations. Phys. Rev. B 65, 165118.

Andrault, D., Bolfan-Casanova, N., Lo Nigro, G., Bouhifd, M., Garbarinho, G., Mezouar, M., 2011. Solidus and liquidus profiles of chondritic mantle: Implication for melting of the Earth across its history. Earth Planet. Sci. Lett. 304, 251–259.

Biggin, A., Strik, G., Langereis, C., 2009. The intensity of the geomagnetic field in the late-Archaean: new measurements and an analysis of the updated IAGA palaeointensity database. Earth Planets Space 61, 9–22.

Braginsky, S., 1963. Structure of the F layer and reasons for convection in the Earth's core. Sov. Phys. Dokl. 149, 8–10.

Braginsky, S., Roberts, P., 1995. Equations governing convection in Earth's core and the geodynamo. Geophys. Astrophys. Fluid Dyn. 79, 1–97.

Buffett, B., 2002. Estimates of heat flow in the deep mantle based on the power requirements for the geodynamo. Geophys. Res. Lett. 29, 10.1029/2001GL014649.

Buffett, B., 2009. Onset and orientation of convection in the inner core. Geophys. J. Int. 179, 711–719.

Buffett, B., 2012. Earth science: Geomagnetism under scrutiny. Nature 485, 319–320.

Buffett, B., 2014. Geomagnetic fluctuations reveal stable stratification at the top of the Earth's core. Nature 507, 484–487.

Buffett, B., Huppert, H., Lister, J., Woods, A., 1996. On the thermal evolution of the Earth's core. J. Geophys. Res. 101, 7989–8006.

Davies, C., Gubbins, D., 2011. A buoyancy profile for the Earth's core. Geophys. J. Int. 187, 549–563.

Davies, G., 2007. Mantle regulation of core cooling: A geodynamo without core radioactivity? Phys. Earth Planet. Int. 160, 215–229.

de Koker, N., Steinle-Neumann, G., Vojtech, V., 2012. Electrical resistivity and thermal conductivity of liquid Fe alloys at high P and T and heat flux in Earth's core. Proc. Natl. Acad. Sci. 109, 4070–4073.

Dziewonski, A., Anderson, D., 1981. Preliminary Reference Earth Model. Phys. Earth Planet. Int. 25, 297–356.

Fiquet, G., Auzende, A., Siebert, J., Corgne, A., Bureau, H., Ozawa, H., Garbarino, G., 2010. Melting of peridotite to 140 gigapascals. Science 329, 1516–1518.

Gomi, H., Ohta, K., Hirose, K., Labrosse, S., Caracas, R., Verstraete, V., Hernlund, J., 2013. The high conductivity of iron and thermal evolution of the Earth's core. Phys. Earth Planet. Int. 224, 88–103.

Gubbins, D., 1975. Can the Earth's magnetic field be sustained by core oscillations? Geophys. Res. Lett. 2, 409–412.

Gubbins, D., 2007. Geomagnetic constraints on stratification at the top of Earth's core. Earth Planets Space 59, 661–664.

Gubbins, D., Alfè, D., Davies, C., 2013. Compositional instability of Earth's solid inner core. Geophys. Res. Lett. 40, 1084–1088.

Gubbins, D., Alfe, D., Masters, G., Price, G., Gillan, M., 2003. Can the Earth's dynamo run on heat alone? Geophys. J. Int. 155, 609–622.

Gubbins, D., Alfe, D., Masters, G., Price, G., Gillan, M., 2004. Gross thermodynamics of two-component core convection. Geophys. J. Int. 157, 1407–1414.

Gubbins, D., Masters, T., Jacobs, J., 1979. Thermal evolution of the Earth's core. Geophys. J. R. Astr. Soc. 59, 57–99.

Hirose, K., Labrosse, S., Hernlund, J., 2013. Compositional state of Earth's core. Annual Review of Earth and Planetary Sciences 41, 657–691.

Jaupart, C., Labrosse, S., Mareschal, J.-C., 2007. Temperatures, heat and energy in the mantle of the Earth. In: Schubert, G. (Ed.), Treatise on Geophysics, Vol. 7. Elsevier, Amsterdam, pp. 254–303.

Labrosse, S., 2003. Thermal and magnetic evolution of the Earth's core. Phys. Earth Planet. Int. 140, 127–143.

Labrosse, S., 2014. Thermal and compositional stratification of the inner core. C. R. Acad. Sci. Paris.

Labrosse, S., Hernlund, J., Coltice, N., 2007. A crystallizing dense magma ocean at the base of the Earth's mantle. Nature 450, 866–869.

Labrosse, S., Poirier, J.-P., Le Moeul, J.-L., 1997. On cooling of the Earth's core. Phys. Earth Planet. Int. 99, 1–17.

Labrosse, S., Poirier, J.-P., Le Moeul, J.-L., 2001. The age of the inner core. Earth Planet. Sci. Lett. 190, 111–123.

Lay, T., Hernlund, J., Buffett, B., 2009. Core-mantle boundary heat flow. Nat. Geosci. 1, 25–32.

Lister, J., 2003. Expressions for the dissipation driven by convection in the Earth's core. Phys. Earth Planet. Int. 140, 145–158.

Lister, J., Buffett, B., 1995. The strength and efficiency of thermal and compositional convection in the geodynamo. Phys. Earth Planet. Int. 91, 17–30.

Lister, J., Buffett, B., 1998. Stratification of the outer core at the core-mantle boundary. Phys. Earth Planet. Int. 105, 5–19.

Loper, D., 1978. Some thermal consequences of a gravitationally powered dynamo. J. Geophys. Res. 831.

Manglik, A., Wicht, J., Christensen, U., 2010. A dynamo model with double diffusive convection for Mercury's core. Earth Planet. Sci. Lett. 209, 619–628.

Masters, G., Gubbins, D., 2003. On the resolution of density within the Earth. Phys. Earth Planet. Int. 140, 159–167.

Nakagawa, T., Tackley, P., 2013. Implications of high core thermal conductivity on Earth's coupled mantle and core evolution. Geophys. Res. Lett. 40, 1–5.

Nakagawa, T., Tackley, P., 2014. Influence of combined primordial layering and recycled MORB on the coupled thermal evolution of Earth's mantle and core. Geochem. Geophys. Geosys. 15, 619–633.

Nimmo, F., 2007. Thermal and compositional evolution of the core. In: Schubert, G. (Ed.), Treatise on Geophysics, Vol. 9. Elsevier, Amsterdam, pp. 217–241.

Nimmo, F., 2014. Energetics of the core. In: Schubert, G. (Ed.), Treatise on Geophysics 2nd Edn, Vol. 9. Elsevier, Amsterdam, pp. 31–65.

Nimmo, F., Price, G., Brodholt, J., Gubbins, D., 2004. The influence of potassium on core and geodynamo evolution. Geophys. J. Int. 156, 363–376.

Nomura, R., Hirose, K., Uesugi, K., Ohishi, Y., Tsuchiyama, A., Miyake, A., Ueno, Y., 2014. Low core-mantle boundary temperature inferred from the solidus of pyrolite. Science 343, 522–524.

Poirier, J.-P., 1994. Introduction to the physics of Earth's interior, 2nd Edition. Cambridge University Press.

Pozzo, M., Davies, C., Gubbins, D., Alfè, D., 2012. Thermal and electrical conductivity of iron at Earth's core conditions. Nature 485, 355–358.

Pozzo, M., Davies, C., Gubbins, D., Alfè, D., 2013. Transport properties for liquid silicon-oxygen-iron mixtures at Earth's core conditions. Phys. Rev. B 87, 014110.

Pozzo, M., Davies, C., Gubbins, D., Alfè, D., 2014. Thermal and electrical conductivity of solid iron and iron-silicon mixtures at Earth's core conditions. Earth Planet. Sci. Lett. 393, 159–164.

Roberts, P., Jones, C., Calderwood, A., 2003. Energy fluxes and ohmic dissipation in the Earth's core. In: Earth's core and lower mantle. Contributions from the SEDI 2000, The 7th Symposium, pp. 100–129.

Stacey, F., 2007. Core properties, physical. In: Gubbins, D., Herrero-Bervera, E. (Eds.), Encyclopedia of Geomagnetism and Paleomagnetism. Springer, pp. 91–94.

Stacey, F., Anderson, O., 2001. Electrical and thermal conductivities of Fe-Ni-Si alloy under core conditions. Phys. Earth Planet. Int. 124, 153–162.

Stacey, F., Loper, D., 2007. A revised estimate of the conductivity of iron alloy at high pressure and implications for the core energy balance. Phys. Earth Planet. Int. 161, 13–18.

Stevenson, D., 1987. Limits on lateral density and velocity variations in the Earth's outer core. Geophys. J. Int. 88, 311–319.

Tarduno, J., Cottrell, R., Watkeys, M., Hofmann, A., Doubrovine, P., Mamajek, E., Liu, D., Sibeck, D., Neukirch, L., Usui, Y., 2010. Geodynamo, solar wind, and magnetopause 3.4 to 3.45 billion years ago. Science 327, 1238–1240.

Verhoogen, J., 1961. Heat balance of the Earth's core. Geophys. J. R. Astr. Soc. 4, 276–281.

Ziegler, L. B., Stegman, D. R., 2013. Implications of a long-lived basal magma ocean in generating Earth's ancient magnetic field. Geochem. Geophys. Geosys. 14, 4735–4742.